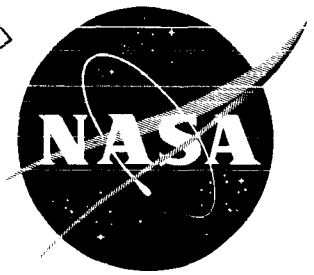

TECHNICAL MEMORANDUM
X-659

THE WIND-INDUCED LOADS ON A DYNAMICALLY SCALED MODEL OF THE DYNA SOAR GLIDER AND TITAN II BOOSTER IN LAUNCH POSITION

By George B. McCullough and Donald A. Buell

Ames Research Center
Moffett Field, Calif.

NATIONAL AERONAUTICS AND SPACE ADMINISTRATION
WASHINGTON
December 1962

[redacted]

NATIONAL AERONAUTICS AND SPACE ADMINISTRATION

TECHNICAL MEMORANDUM X-659

THE WIND-INDUCED LOADS ON A DYNAMICALLY SCALED MODEL OF THE DYNA SOAR GLIDER AND TITAN II BOOSTER IN LAUNCH POSITION*

By George B. McCullough and Donald A. Buell

SUMMARY

The effects of ground winds on the Dyna Soar glider and Titan II booster in the launch position were simulated in wind-tunnel tests of a 6.6-percent scale model. Reynolds numbers up to 5 million, based on the diameter of the booster, simulated ground winds up to 50 miles an hour on the full-scale vehicle. Measurements were made of the base bending moments, torsional loads, and average drag of the model for the complete range of wind directions with respect to the glider.

Two critical wind directions were found to produce substantial lateral dynamic response. A wind direction of 67° to the lower surface of the glider wing was considered the more important because with the wind from this direction, the model also experienced a large static bending load. The dynamic torsional loads were found to be small. Surface roughness, external conduits, and open exhaust ports increased the streamwise average bending loads, and the conduits and open exhaust ports increased the lateral oscillatory bending loads. The presence of an umbilical tower upstream and to one side of the model sharply increased the oscillatory loads, but had small effect on the static loads.

The measured loads are not extrapolated to full scale, but such an extrapolation could be made with knowledge of the structural characteristics of the full-scale vehicle.

INTRODUCTION

The action of wind on tall, cylindrical structures, such as smokestacks, has long been known to induce oscillations in the plane

*Title, Unclassified

[redacted]

perpendicular to the wind as well as drag loads in the streamwise direction. In some cases the lateral oscillations have been large enough to cause smokestacks to fail. The study of wind-induced oscillatory loads has recently been focused on the problem of defining the structural loading and response of large missiles on the launch pad when subjected to natural winds prior to launch. Since the crossflow Reynolds number of a large-diameter cylinder in any appreciable breeze is supercritical (i.e., above the region of the periodic Von Kármán vortex discharge), the reasons for the lateral response are not entirely clear. To date there is no known method for predicting the magnitude of the response. The lack of a theoretical method for predicting the loads due to winds has forced recourse to wind-tunnel experiments with dynamically scaled models. One such investigation is reported in reference 1 where, for some conditions, it was found that the lateral bending stresses were several times the dragwise bending stresses. Since the missile represented in this investigation is axisymmetric, as are missiles, in general, the possibility of significant torsional loads being induced was not considered. With the advent of a proposed glider-type vehicle with an exposed wing mounted on top of a tall cylindrical booster, wind-induced torsional oscillations appeared to be a definite possibility. Furthermore, the relatively large flat area of the glider wing when broadside to the wind appeared to be a source of high streamwise bending loads at the base of the booster, particularly in gusty conditions. To investigate the importance of torsional oscillations and to measure the steady and oscillatory bending loads, a 6.6-percent scale model of the Dyna Soar glider with Titan II booster and its umbilical tower was supplied by The Martin Company. The model was tested in the Ames 12-Foot Pressure Wind Tunnel as part of the NASA program supporting the Dyna Soar Project of the U.S. Air Force. The purpose of this report is to present the results obtained.

NOTATION

C_D drag coefficient, positive downwind, $\frac{\text{drag}}{qS}$

C_Y lateral force coefficient, positive to left looking downwind, $\frac{\text{lateral force}}{qS}$

N yawing moment, positive clockwise looking down from above, ft-lb

L lateral overturning moment measured by wind-tunnel balance, positive counterclockwise looking downwind, ft-lb

S frontal area, 7.354 sq ft (see fig. 1)

q dynamic pressure, lb/sq ft

The origin of bending moments and lateral overturning moment is station 12 as shown in figure 1(a).

The origin of yawing moment is the longitudinal axis of the booster.

MODEL AND INSTRUMENTATION

Model

Sketches of the 0.066 scale model of the Dyna Soar glider and Titan II booster are shown in figure 1. The glider angle convention and the umbilical tower position are shown in figure 2. Photographs of the model installed in the wind tunnel are shown in figures 3 and 4.

The cylindrical portion of the model was made of aluminum in four sections bolted together. Each of the three upper sections consisted of an outer tube and eight internal longitudinal stringers welded to bulkheads at the ends of the tubular sections. This type of construction produced the desired relationship between bending and torsional stiffness. Inside each of the two upper sections was a steel-encased lead weight. The flanged base section was solid.

Attached to the upper end of the top section was a short truncated cone ending in a hollow steel spindle about which the glider could rotate on two roller bearings as shown in the schematic diagram of figure 1(c). The glider was restrained in rotation by a steel torsion bar which extended through the hollow spindle. The upper end of the torsion bar was attached to the glider, and the lower end to a motor-driven gear set housed within the conical section. Backlash in the gear set could be eliminated by locking the gear with a friction-type clamp. Also, a greater amount of torsional stiffness could be obtained by locking the glider directly to the spindle with a second clamp. This condition more nearly simulated the torsional stiffness of the full-scale vehicle; consequently, most of the tests were made with the glider locked to the spindle although torsion bars of three degrees of stiffness were provided.

The glider model was made of aluminum and wood. The transition section from the base of the glider to the top of the booster was integral with the glider, and the entire assembly slipped over the spindle and covered the conical spindle support. A sketch of the glider and transition section is shown in figure 1(d). A remote motor control and angular position indicator permitted the glider to be rotated with the wind tunnel running, but because of the backlash in the gear set, this system was used only to find the critical glider angles. Otherwise, the gear set or the glider was locked manually after the glider had been set to the desired angle.

Near the bottom end of the model was a set of cruciform fins welded to a collar which slipped over the base section. The two pairs of fins were of unequal area and span. The normal arrangement is with the larger pair of fins parallel with the wing plane of the glider. Their effects on the measurements were small and in order to expedite the tests this normal orientation was not always maintained.

The tubular section of the model contained a circumferential row of 20 equally spaced holes, 17/32 inch in diameter, as shown in figure 1. These holes represented open exhaust ports for the second-stage motor of the booster. The model was also tested with the holes plugged and smoothly faired.

The external conduits on the full-scale vehicle were simulated by wood slats glued and screwed to the cylindrical portion of the model. The slats were on opposite sides of the model in a plane rotated 60° to the plane of symmetry of the glider as shown in figure 1(b).

Surface roughness on the booster was simulated by nine vertical strips of cellulose tape, 1/2 inch wide and 0.003 inch thick. The tape was applied every 22-1/2° over the upstream half of the two upper section of the booster. The roughened condition is referred to as "tapes," whereas the model without tapes, conduits, or holes is referred to as "clean."

A table of model weights and weight distribution is shown in figure 5.

Model Instrumentation

The model was instrumented with strain gages bonded to the inside of the aluminum tube about 2 inches above the base section. The gages were 90° apart so as to respond to bending in the streamwise and lateral planes. Torsion gages were bonded to the torsion bars and to the base of the glider support spindle.

The gages were powered by 20-kilocycle carrier current; the output signals of the gages were amplified and displayed on oscilloscopes for visual observation. The outputs were also recorded simultaneously on an oscillograph and on a digital printer. The digital printer recorded averaged values obtained from the signals passed through a capacitive-resistive network.

An accelerometer was temporarily attached to the glider to measure the amplitude of the oscillations at the tip during calibration of the model. A hand-held velocity probe placed against various stations along the model was used to obtain model mode shape.

CALIBRATIONS

After installation in the wind tunnel, the model was pulled in the streamwise and lateral directions with known loads to calibrate the bending moment gages near its base. The moment center was the joint between the solid base section and the bottom tubular section (station 12 in fig. 1(a)).

A known couple was applied to the torsion members to calibrate the torsion gages on the stiff torsion bar and on the spindle support.

For the dynamic calibrations the model was shaken in the streamwise and in the lateral directions with an electromagnetic shaker which excited the model principally in the first bending mode. To determine the natural frequency and the damping of the model the power to the shaker was cut and the decay of the bending moment trace on the oscillograph record was measured. The connection between the shaker and the model added some mass to the system, and the flexures of the shaker head added some external damping, but these effects were not believed to be significant.

Attempts to determine the torsional damping of the glider restraint were not entirely successful. Values of damping ranging from 1 to 4 percent of critical were obtained.

Plots of the damping and mode shapes are shown in figures 6 and 7. Other model characteristics are given in table I.

TESTS AND MEASUREMENTS

Two different types of tests were performed to establish the loads caused by simulated ground winds. Structural response or "dynamic" tests were performed with the model bolted to a 4-inch-thick steel plate which in turn was bolted to the tunnel structure. The data were obtained from the outputs of the strain gages in the model. For these tests the tubular portion of the model remained fixed relative to the airstream. To simulate different flow directions the glider and fins were rotated, and the conduits relative to the tubular portion of the model were repositioned. Thus, the strain gages were always properly oriented to measure bending moments parallel and normal to the relative wind. The outputs of the torsional gages were recorded by the same equipment mentioned previously. Two-minute data records were taken at successively increased tunnel speeds until one of the monitoring oscilloscopes indicated that the design load limit had been reached.

After the dynamic data had been obtained, the model was mounted on the turntable of the six-component force balance system of the wind tunnel to obtain the steady-state forces and moments acting on the model. (Dynamic measurements cannot be made on the balance because of the extraneous damping introduced by the model support.) With this system the

entire model can be rotated through an angle range of 40°. Rotating the glider and repositioning the conduits and fins on the booster in increments of 40° allowed the entire range of wind angles to be covered. For the model to rotate it was necessary to leave a small annular gap between the model and the fairing covering the base of the model. A few measurements were made with this gap sealed by a rubber dam to assess the effect of air leakage through the gap.

All tests were made with a tunnel static pressure of 4.7 atmospheres (average density, 0.0112 slug/cu ft). The relationship between tunnel dynamic pressure, air velocity, and Reynolds number based on the 7.90-inch diameter of the booster is shown in figure 8.

RESULTS AND DISCUSSION

Dynamic Measurements

Measurements made with this and other similar models have indicated that the oscillatory bending moments are primarily in the first cantilever mode. It was found that the oscillatory torsional moments were small; in fact, for most cases the signal was not much above the noise level. For this reason the dynamic torsional measurements are not presented.

The first objective was to determine the glider angle or angles which resulted in the maximum oscillatory base bending moments. Figure 9 shows the measured maximum peak-to-peak values of the oscillograph trace from the lateral bending-moment gage as the glider was rotated slowly from 0° to 360° and back to 0°. Since the fins at the base of the model could not be rotated remotely, the fins were fixed at 0°. Because of the aerodynamic load on the glider drive mechanism, the tests were made at low speed (dynamic pressure, 75 lb/sq ft; Reynolds number, 2.3 million). It can be seen that peaks occurred in the vicinity of 70°, 160°, 200°, and 290°. Since the 160° and 290° angles were images of 200° and 70°, only the latter two angles were investigated in detail. Short tests were made at higher speeds with the glider fixed at various angles in the vicinity of 70° and 200°. These tests resulted in the selection of 74° and 203° as the critical angles for the investigation of the effects of conduits, exhaust ports, surface roughness, and the presence of the umbilical tower.

Glider angle 203°.- The oscillatory and average bending moments for two practically identical model configurations are shown in figures 10(a) and (b). The differences in model dynamics with different torsion bars and the glider locked are negligible; hence, the differences in bending moments should not be attributed to the differences in torsion bars. These figures are introduced to give an idea of the repeatability of the dynamic data. As mentioned previously, the tests were made at constant

air density, so that the variation of Reynolds number was achieved by varying the tunnel air velocity. Previous investigations of this type have shown similar repeatability of the dynamic data, and have demonstrated that the significance of individual points should be judged only as they affect general trends. Experience has shown that trends in the data can be counted upon to repeat with reasonable consistency.

Although the largest lateral oscillatory bending moments were encountered with a glider angle of 74°, larger total loads (average plus oscillatory) were encountered with a glider angle of 203°. For this reason, a glider angle of 203° was chosen for the investigation of model surface conditions. These effects are shown in figure 11 for the model with the glider locked and the fins in the proper position. For the lower Reynolds numbers there were no great differences in the oscillatory lateral bending moments, but for the higher Reynolds numbers above 4.2 million the model with the exhaust ports open produced the largest bending moments (fig.11(a)). All types of surface roughness increased the average streamwise bending moments (fig. 11(b)), with the conduits having the greatest effect.

In this connection, it should be mentioned that the static and the dynamic model data do not necessarily scale up by the same factor. For cases where the model damping is small compared to the damping of the full-scale vehicle, the dynamic data will scale up by a smaller factor than will the static data. Such is the case in this instance. (The problem of scaling is discussed in ref. 2.) Hence, for equal magnitudes at model scale, the predicted full-scale static loads will be larger than the predicted full-scale dynamic loads.

Glider angle 74°.- The bending moment response of the clean model with the glider at 74° is shown in figure 12. Somewhat greater oscillatory lateral response was evidenced with the stiff torsion bar and gear locked (glider torsional frequency 105 cps) than with the glider locked (frequency 150 cps). This change in torsional frequency had little effect on the streamwise bending moments or on the average bending moments.

Effect of umbilical tower.- The geometric relationship of the umbilical tower, glider, and fins in the proposed launching situation is shown in figure 2. The effect of the introduction of the umbilical tower in this relationship (tower 29°, glider and fins 74°) is shown in figure 12. The lateral oscillatory bending moments were markedly increased with only a small increase in the streamwise oscillatory bending moments. The average bending moments were relatively unaffected.

To achieve other wind directions in the wind tunnel and still maintain the correct tower-vehicle relationship would involve moving the tower. In the investigation reported in reference 1 it was found that a tower position directly upstream of the missile reduced the loads

on the missile; therefore this position was not considered. Tower positions farther to the side of the vehicle were prohibited in the present case because of the close proximity of the tunnel walls. Hence, only the one wind direction for the correct tower-vehicle relationship was investigated. As a matter of interest, however, the glider was rotated to other angular positions with the tower in the 29° position and the fins set at 0°. The stiff torsion bar was used for these tests, but the glider and gear were not locked. Because of the backlash in the gears, the data are not comparable with data obtained with the glider or gear locked.

Figure 13 shows the effect of the tower with the glider at 203°. Although the general levels of the oscillatory bending responses were reduced below those with the glider locked (fig. 12), the effect of the tower was to nearly double the oscillatory response of the model without the tower, glider unlocked. Figure 14 shows a comparison of oscillatory bending moments for the model with the glider positioned at 0°, 203°, and 344°. The angle 344° was selected because the tower is then 45° counterclockwise from the plane of symmetry of the glider, whereas with the glider at 74° the tower is 45° clockwise from the plane of symmetry. The angle of the wind with respect to the wing plane of the glider is, however, different in the two cases. The differences in response are due to glider rotation alone. Of these three angles, the 203° position resulted in larger oscillatory lateral bending moments throughout most of the Reynolds number range.

Static Loads Measurements

Effects of glider angle.- The variations of the drag coefficient C_D and the lateral force coefficient C_Y with glider (and fin) angle from 0° to 220° are shown in figure 15(a). The data are for the model with the exhaust ports open and with the conduits installed in their proper angular relationship to the glider. The Reynolds number was about 4.5 million (q = 300 lb/sq ft). It might be expected that maximum drag would occur at 0° and 180°, instead of at 10° and 190°. The skewness of the curve is probably due to the asymmetric location of the conduits with respect to the glider. The minimum drag occurred at about 90° where the glider wing plane and large pitch fins were parallel to the wind. The magnitude of the lateral force was much less than that of the drag force, as would be expected, and must be due to the lateral lifting force on the glider wing and fins, and to the presence of the conduits on the cylindrical booster.

Figure 15(b) shows the corresponding variation of N/q (yawing moment divided by dynamic pressure) with glider angle. The yawing moment is not zero at 0° and 180°, probably because of small asymmetries of the model. The maximum yawing moment occurred with the glider wing and pitch-fin planes inclined about 30° to the wind stream.

The movement of the center of pressure of the streamwise loads computed from balance measurements is small, dropping down about 5 inches as the glider wing plane becomes parallel with the wind (fig. 15(c)). The corresponding lateral center of pressure is not presented because the computed values were erratic due to the small magnitude and sign reversals of the lateral force in portions of the angle range. Instead, the variations of L/q (the lateral overturning moment divided by dynamic pressure) are presented in figure 15(d).

Effect of conduits and exhaust ports.- The effects of conduits and the exhaust ports for the glider angle range from 180° to 220° are shown in figure 16. In general, the effect of adding the conduits to the booster was to increase both the drag and the side force. Opening the exhaust ports, however, had but little effect (fig. 16(a)). The conduits and exhaust ports had no effect on yawing moment (fig. 16(b)), or on the streamwise center of pressure (fig. 16(c)), but increased the lateral overturning moment throughout most of the angle range (fig. 16(d)).

A similar effect of conduits and the exhaust ports for the glider angle range from 0° to 40° is shown in figure 17. These angles were selected because they encompass the regions of maximum drag and lateral force.

Effect of Reynolds number.- The effect of Reynolds number on the characteristics of the model with conduits installed, exhaust ports open, and glider and fin angle 200° is shown in figure 18. For this test the annular gap in the fairing around the base of the model was sealed. In general, the effects of Reynolds number are small. Also shown are points from figure 15 for the same configuration without the seal. The agreement between the data with the model sealed and unsealed is good except for the lateral force which was smaller with the model sealed. A portion of the difference could be due to small differences in the glider and fin angle settings. It can be concluded, however, that the air leakage around the base of the model mounted on the wind-tunnel balance did not significantly affect the data.

The drag coefficient measured in the present investigation agreed well with that in an earlier but unpublished investigation of the Dyna Soar glider on the Titan I booster, in which no attempt was made to simulate or measure torsional characteristics. The greatest lateral oscillatory response was with a glider angle of 200°, which compares well with the 203° angle of the present investigation. A critical angle in the vicinity of 74° was not found, however. The failure of the Titan I model to respond at this angle may have been due to its greater torsional rigidity.

CONCLUSIONS

Simulated ground-wind tests have been performed on a 6.6-percent scale model of the Dyna Soar glider with Titan II booster in the launch position. Reynolds numbers up to 5×10^6, based on the diameter of the booster, were obtained which correspond to ground winds up to 50 miles per hour on the full-scale vehicle. The following results, which apply at model scale, were obtained:

1. The oscillatory torsional response of the model was small for torsional stiffness representative of the full-scale vehicle.

2. Two critical glider angles were found to result in relatively large oscillatory lateral bending moments. The larger response was with a glider angle of 74° (wind direction 16° from the upper surface of the glider wing). The next larger lateral response was with a glider angle of 203° (wind direction 67° from the lower surface of the glider wing). The latter angle was considered more critical because of the large average streamwise bending moments with the glider nearly broadside to the wind.

3. Surface roughness, external conduits, and open exhaust ports increased the streamwise average bending loads, and the conduits and open exhaust ports increased the lateral oscillatory bending loads.

4. The presence of an umbilical tower upstream and to one side of the model sharply increased the oscillatory lateral bending moments, but had no effect on the average streamwise bending moments.

Ames Research Center
National Aeronautics and Space Administration
Moffett Field, Calif., July 23, 1962

REFERENCES

1. Buell, Donald A., and Kenyon, George C.: The Wind-Induced Loads on a Dynamically Scaled Model of a Large Missile in Launching Position. NASA TM X-109, 1959.

2. Ezra, A. A., and Birnbaum, S.: Design Criteria for Space Vehicles to Resist Wind Induced Oscillations. The Martin Co. (Presented at Structural Design and Space Vehicles Conference, Santa Barbara, Calif., April 6-8, 1960), American Rocket Society Paper 1081-60.

TABLE I.- MODEL CHARACTERISTICS

Streamwise damping, ratio to critical	0.0028
Streamwise natural frequency	17.5 cps
Lateral damping, ratio to critical	0.0051
Lateral natural frequency	17.6 cps
Torsional frequency, glider locked	150 cps
Torsional stiffness, glider locked	0.0005°/ft-lb
Torsional frequency, stiff bar, gear locked	105 cps
Torsional stiffness, stiff bar, gear locked	0.0053°/ft-lb
Bending moment per unit tip deflection	220,000 in.-lb/in.

[redacted]

[redacted]

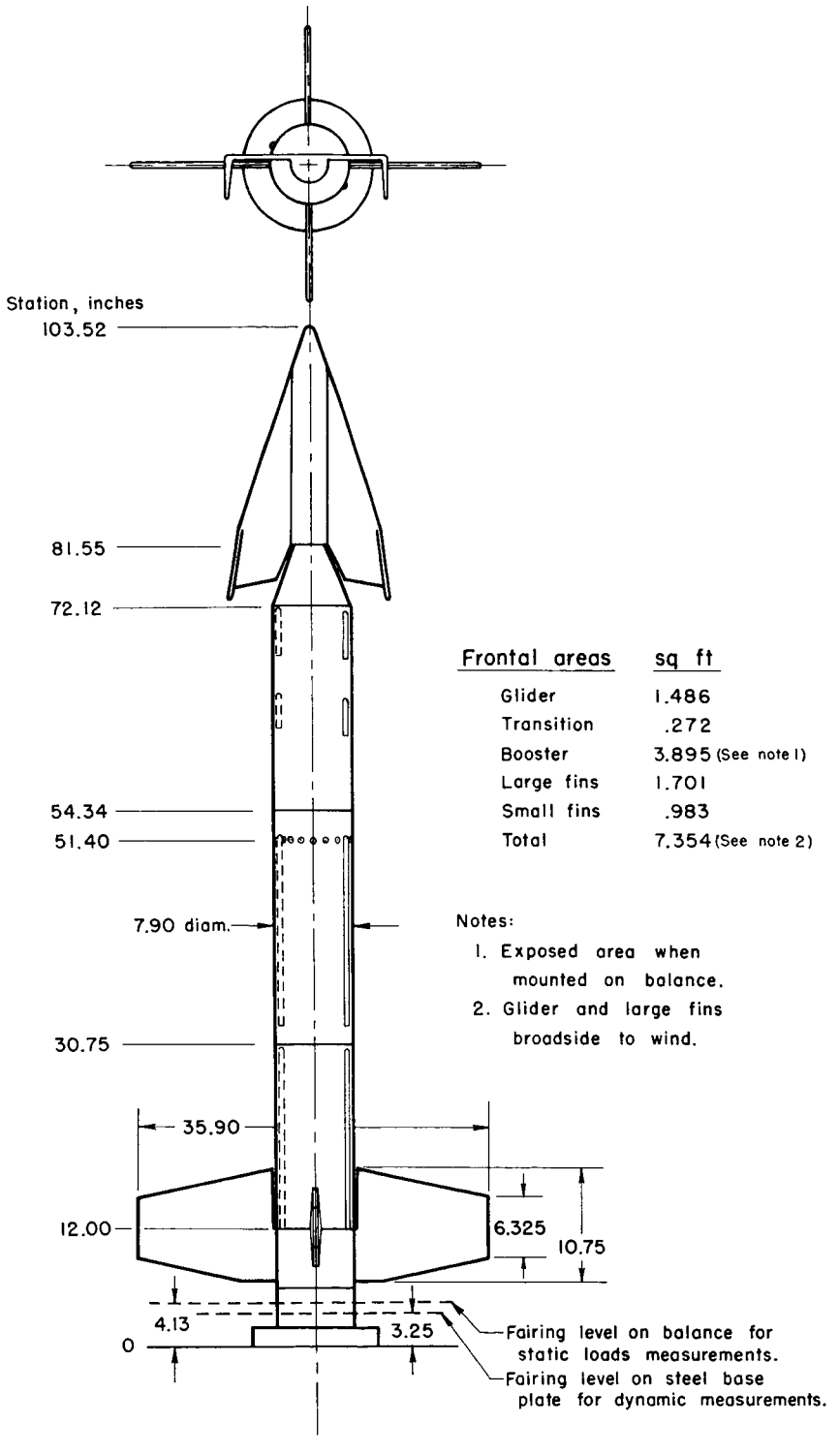

(a) Front view.

Figure 1.- Sketch of model.

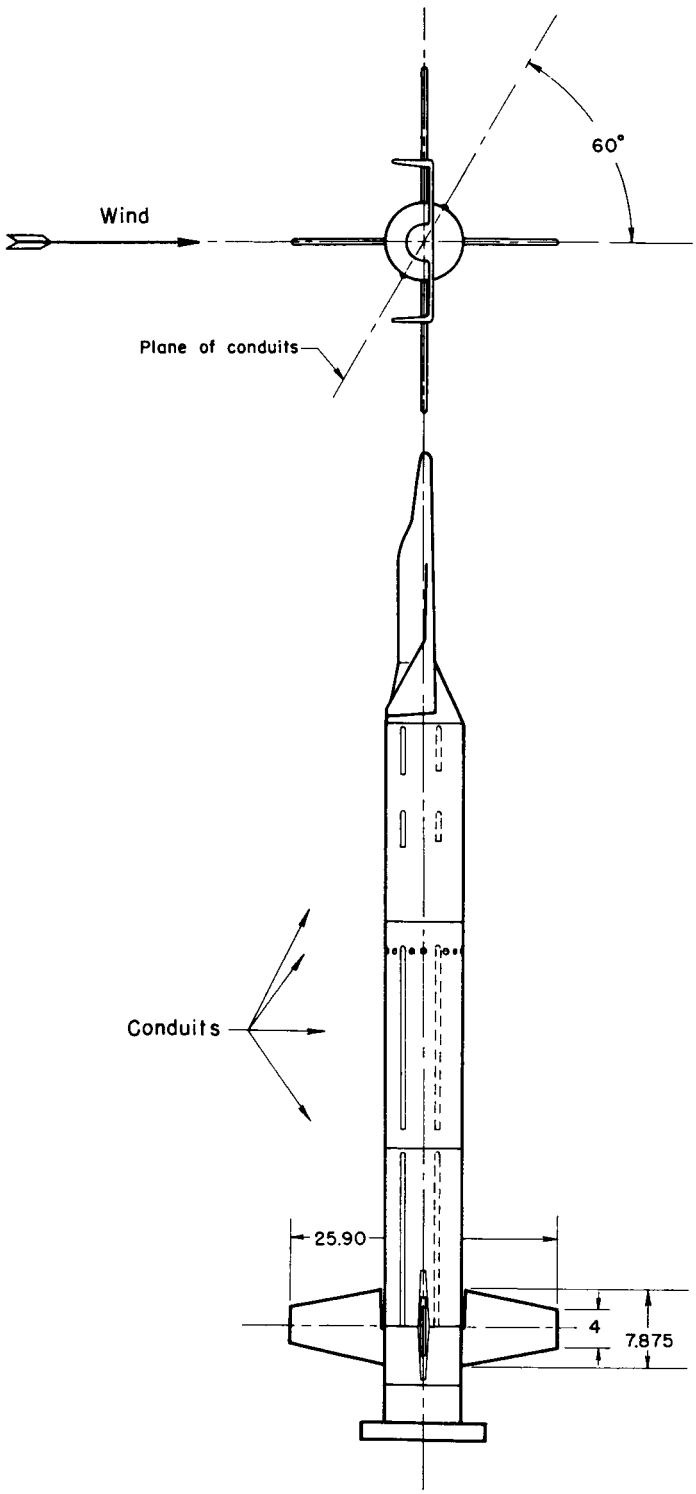

(b) Side view; glider angle 0°.

Figure 1.- Continued.

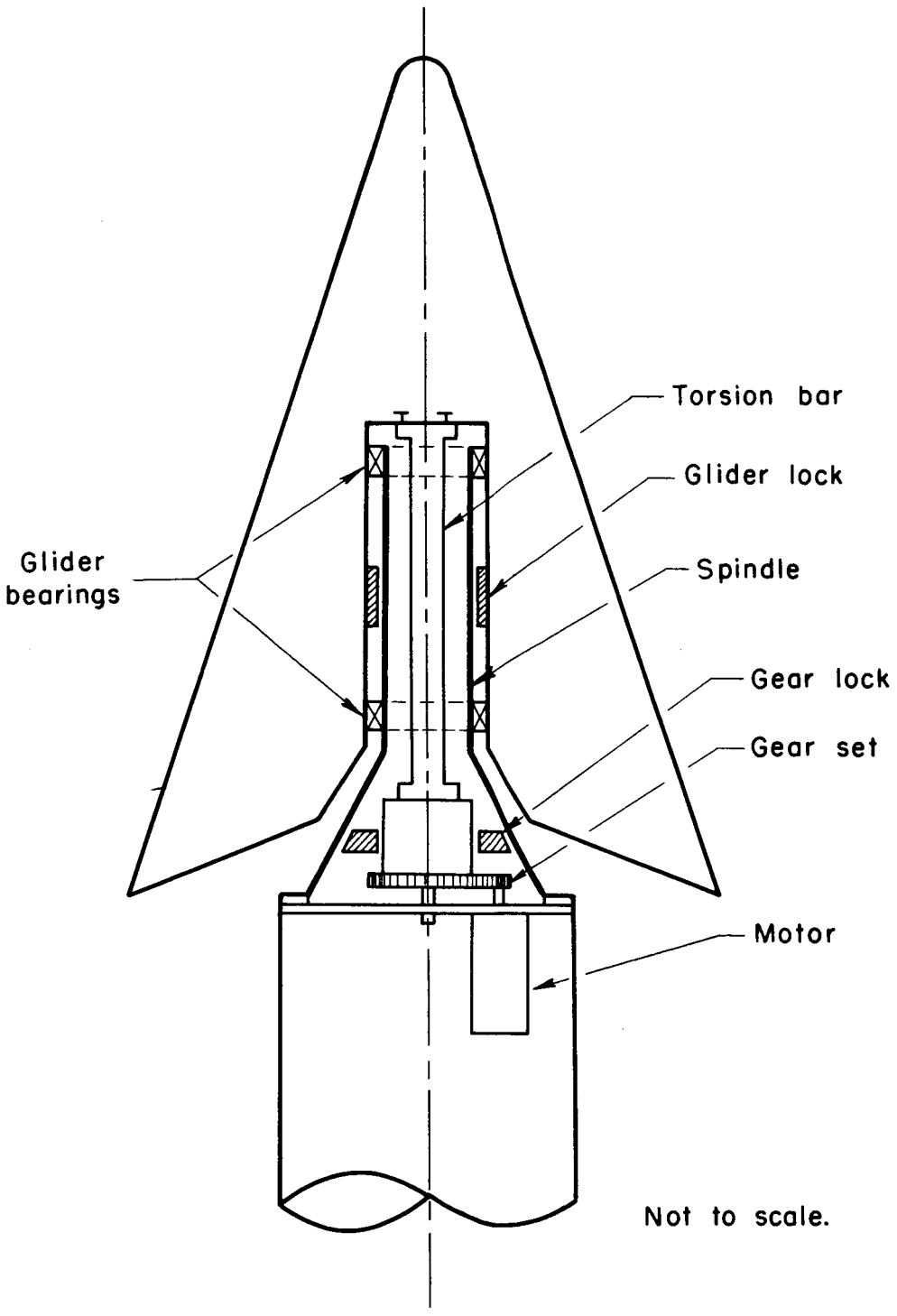

(c) Schematic diagram of glider support.

Figure 1.- Continued.

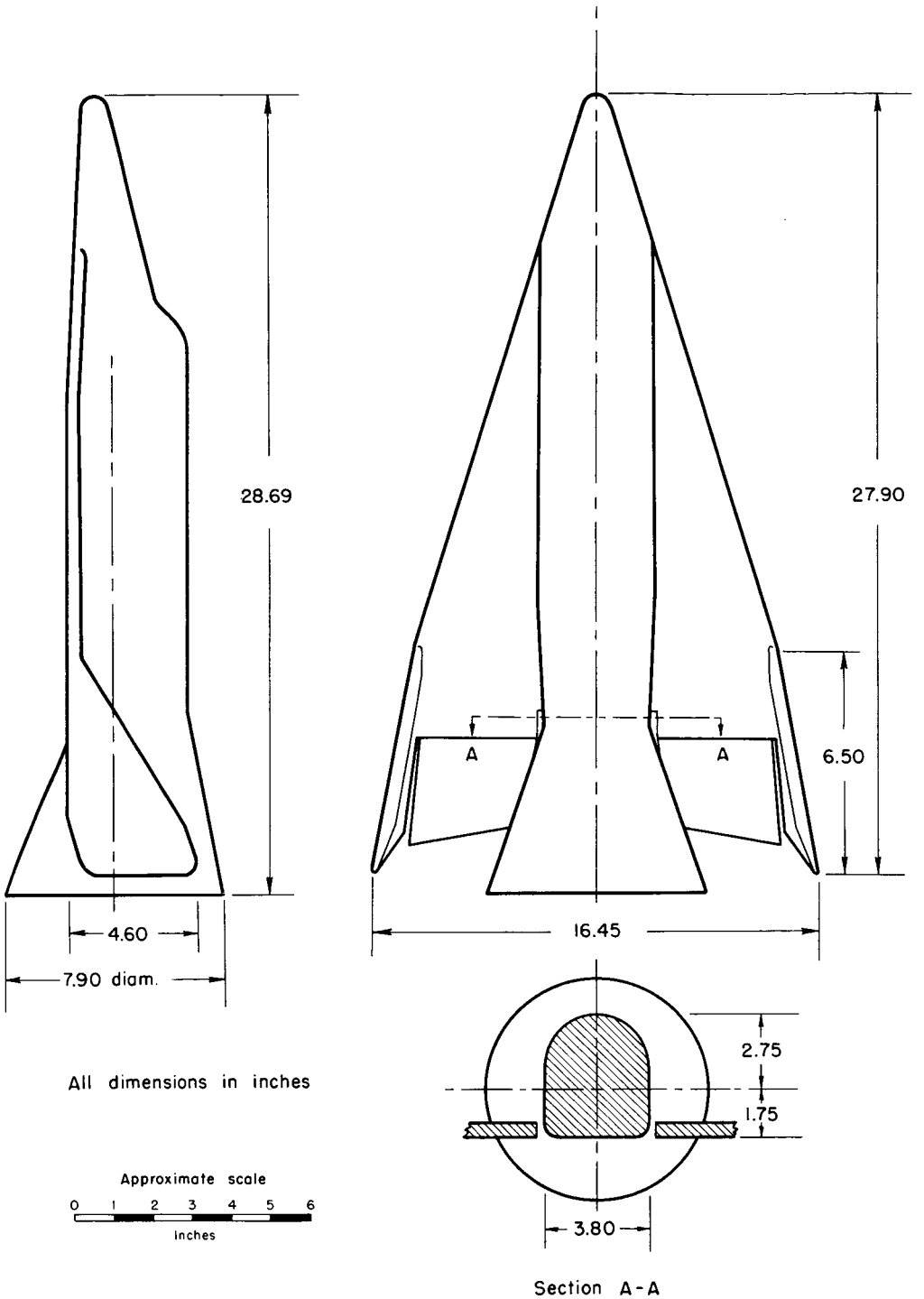

(d) Sketch of glider and transition.

Figure 1.- Concluded.

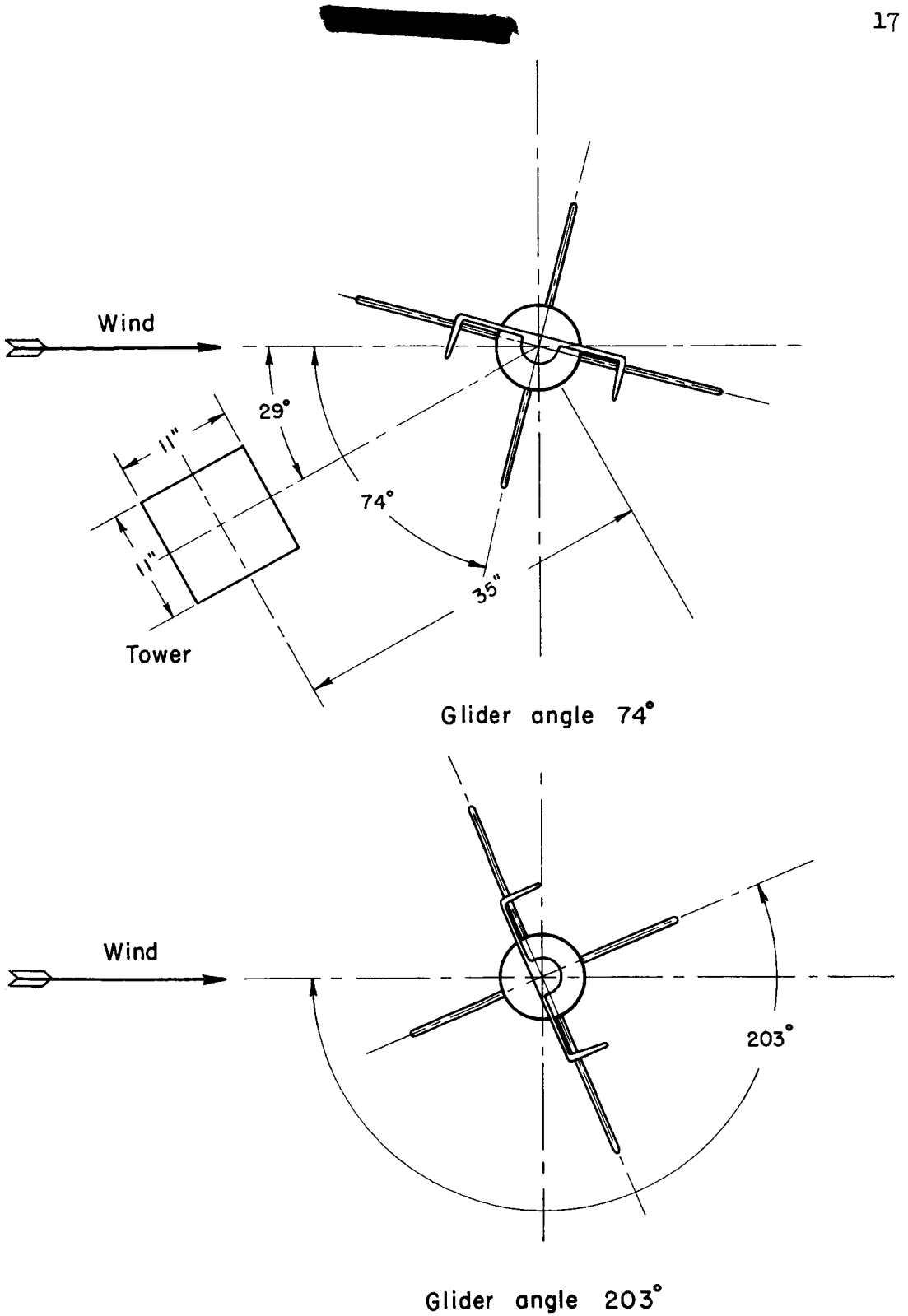

Figure 2.- Plan views of model showing glider angle convention and tower location.

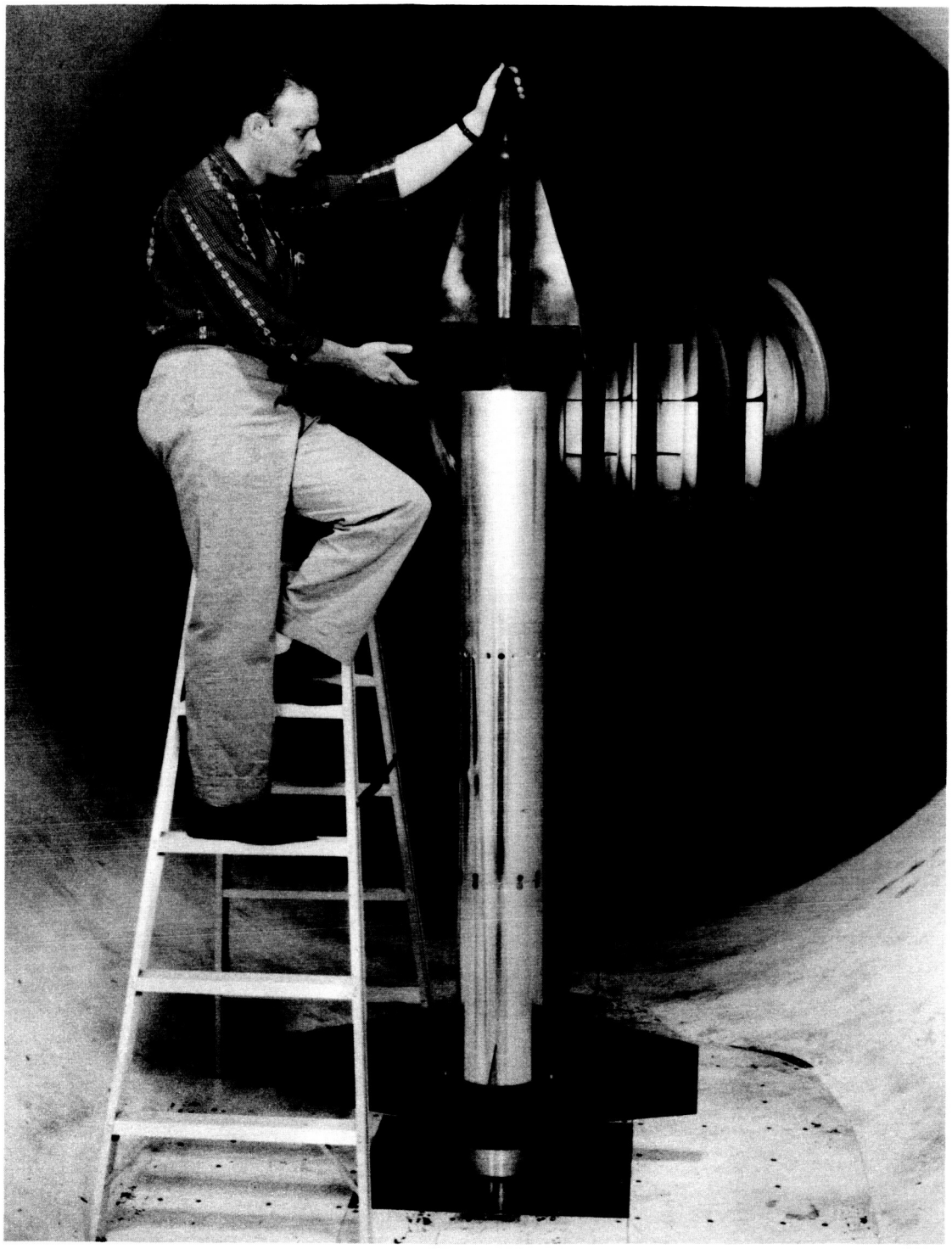

A-27903

Figure 3.- Model in wind tunnel; exhaust ports open, no conduits.

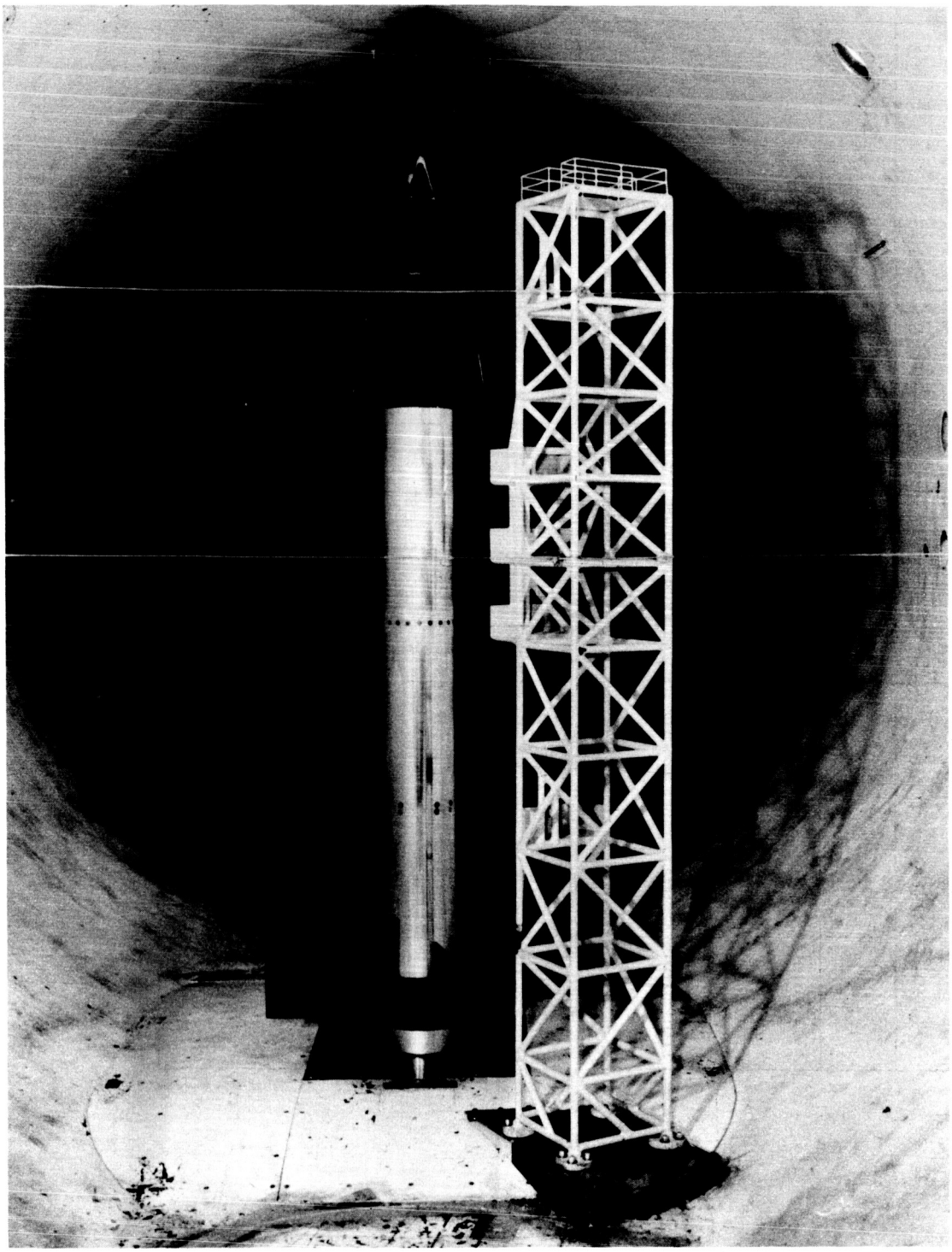

A-28042

Figure 4.- Model and umbilical tower installed in wind tunnel.

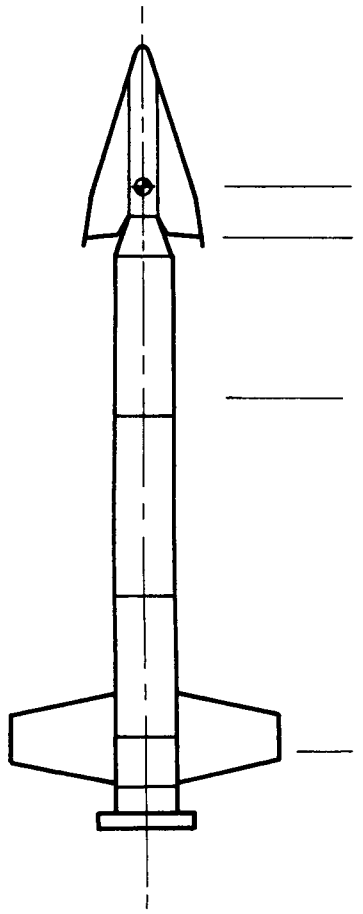

Concentrated mass		
Item	Weight, lb	Station, in.
Glider	22.0	87.92
Transition	32.5	77.98
Ballast	56.0	57.28
Fins	12.5	10.3

Distributed mass			
Item	Weight, lb	lb/in.	Station, in.
Section	12.0	0.86	74.79 – 60.78
Section & Ballast	192.5	8.27	53.78 – 30.75
Section	24.0	1.28	30.75 – 12.00
Base	70.0	5.83	12.00 – 0

Total weight 421.5 lb

Figure 5.- Model weight distribution.

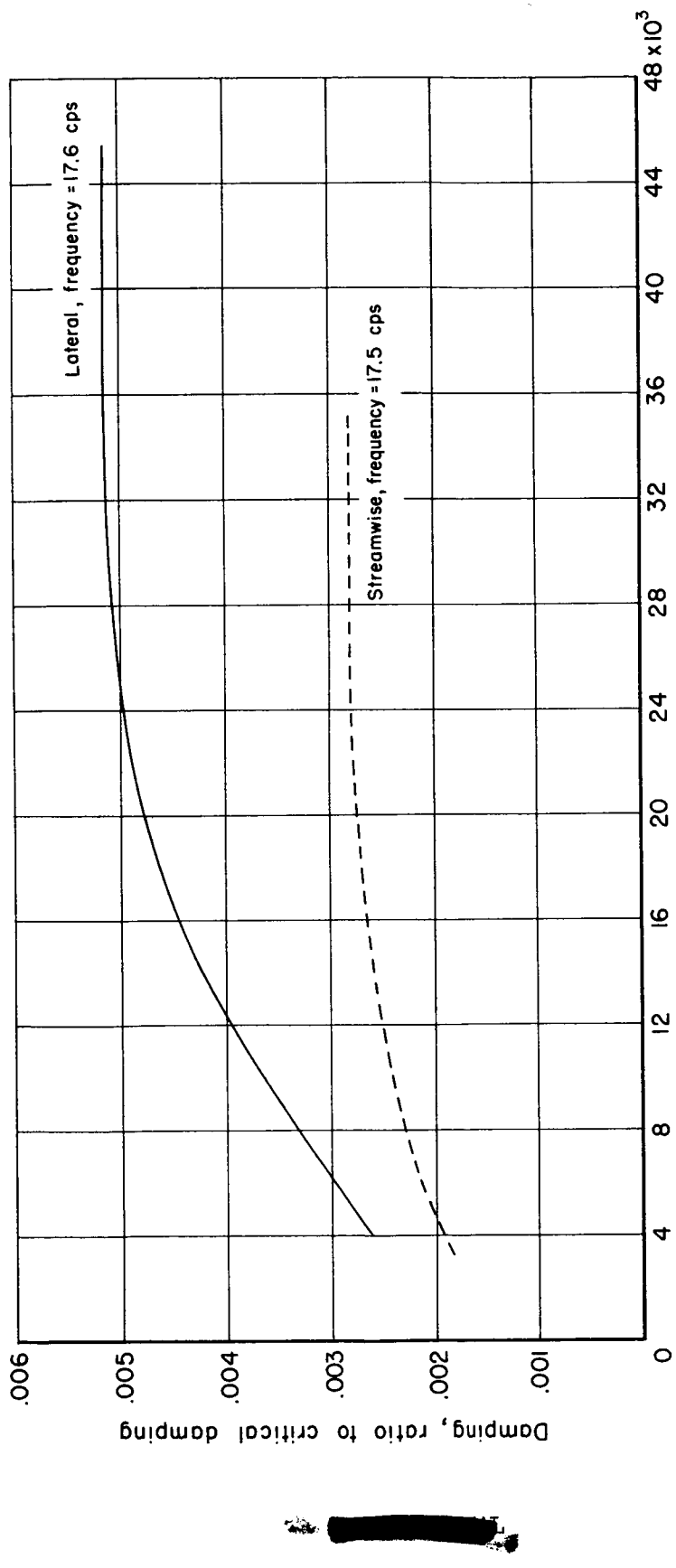

Figure 6.- Damping in the lateral and streamwise directions.

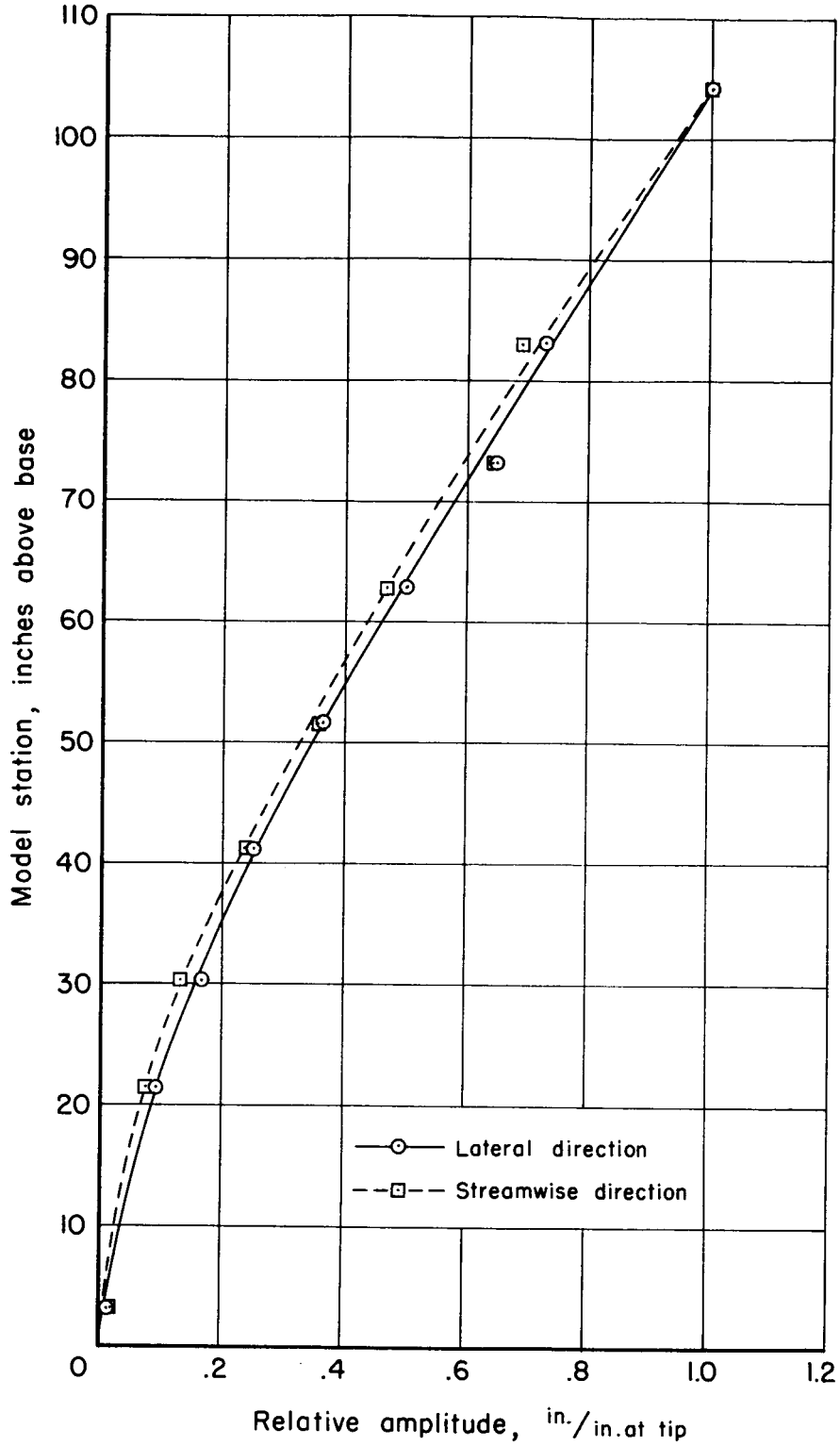

Figure 7.- Mode shape in the lateral and streamwise directions.

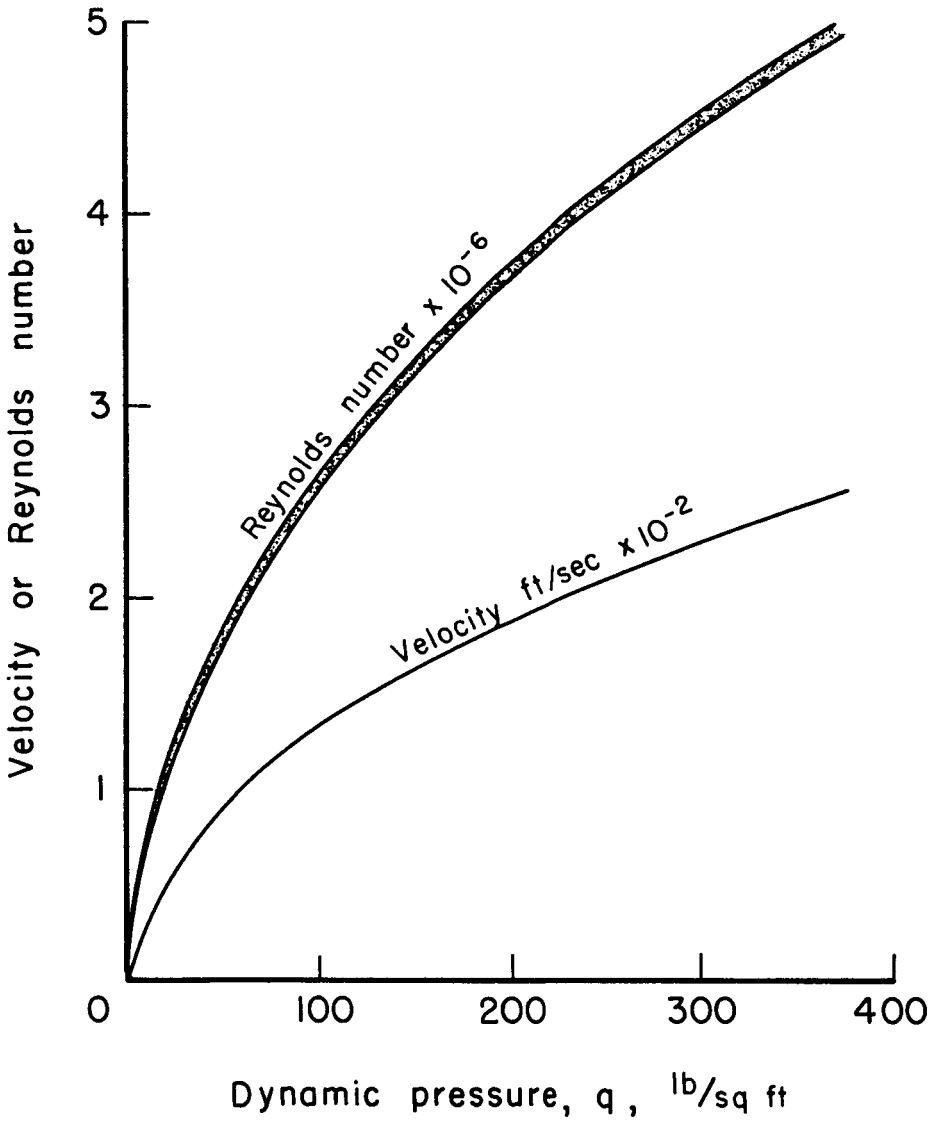

Figure 8.- The variation of Reynolds number and velocity with dynamic pressure.

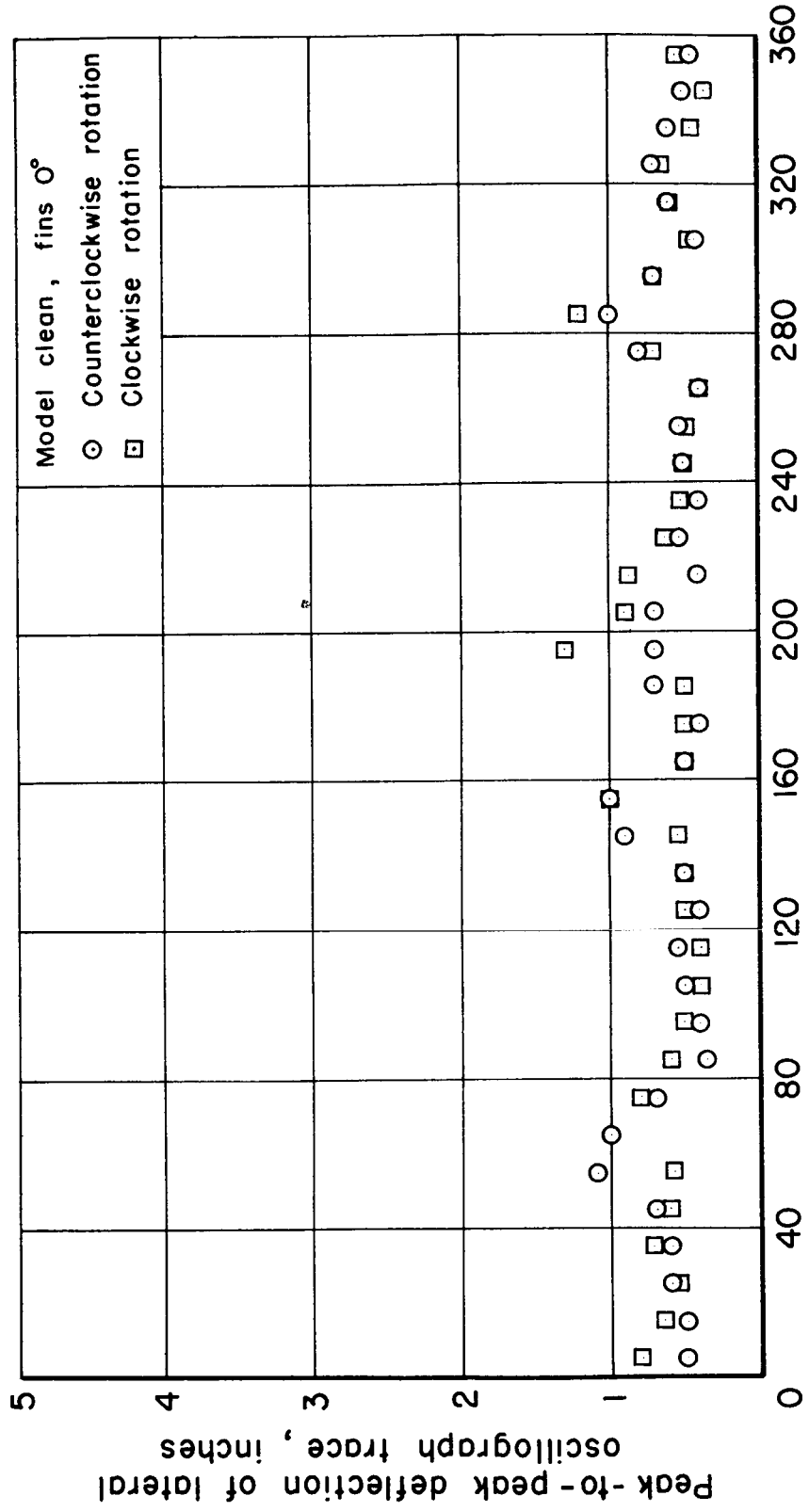

(a) Model clean.

Figure 9.- Lateral oscillograph trace deflection as glider was rotated.

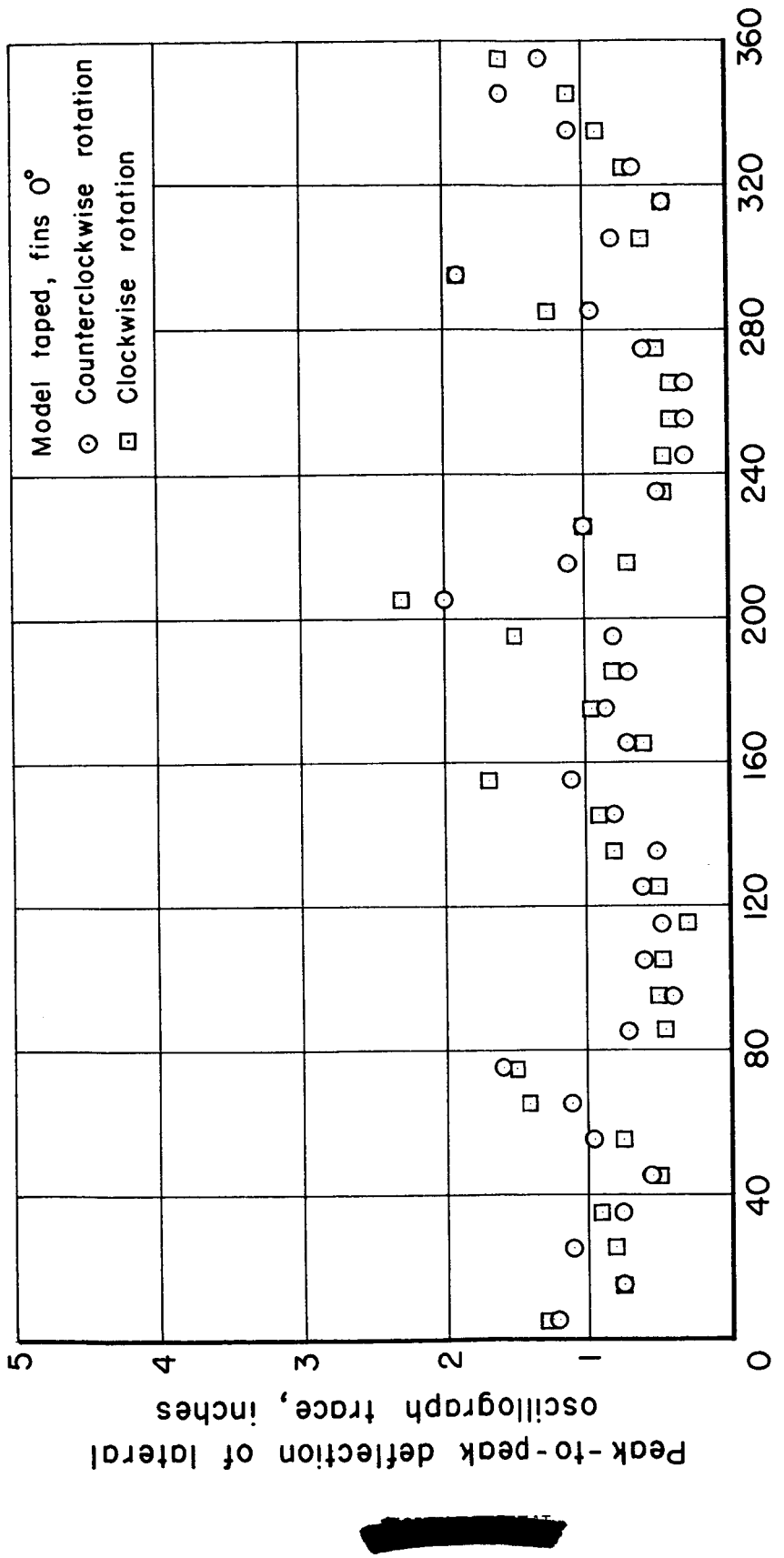

(b) Model taped.

Figure 9.- Concluded.

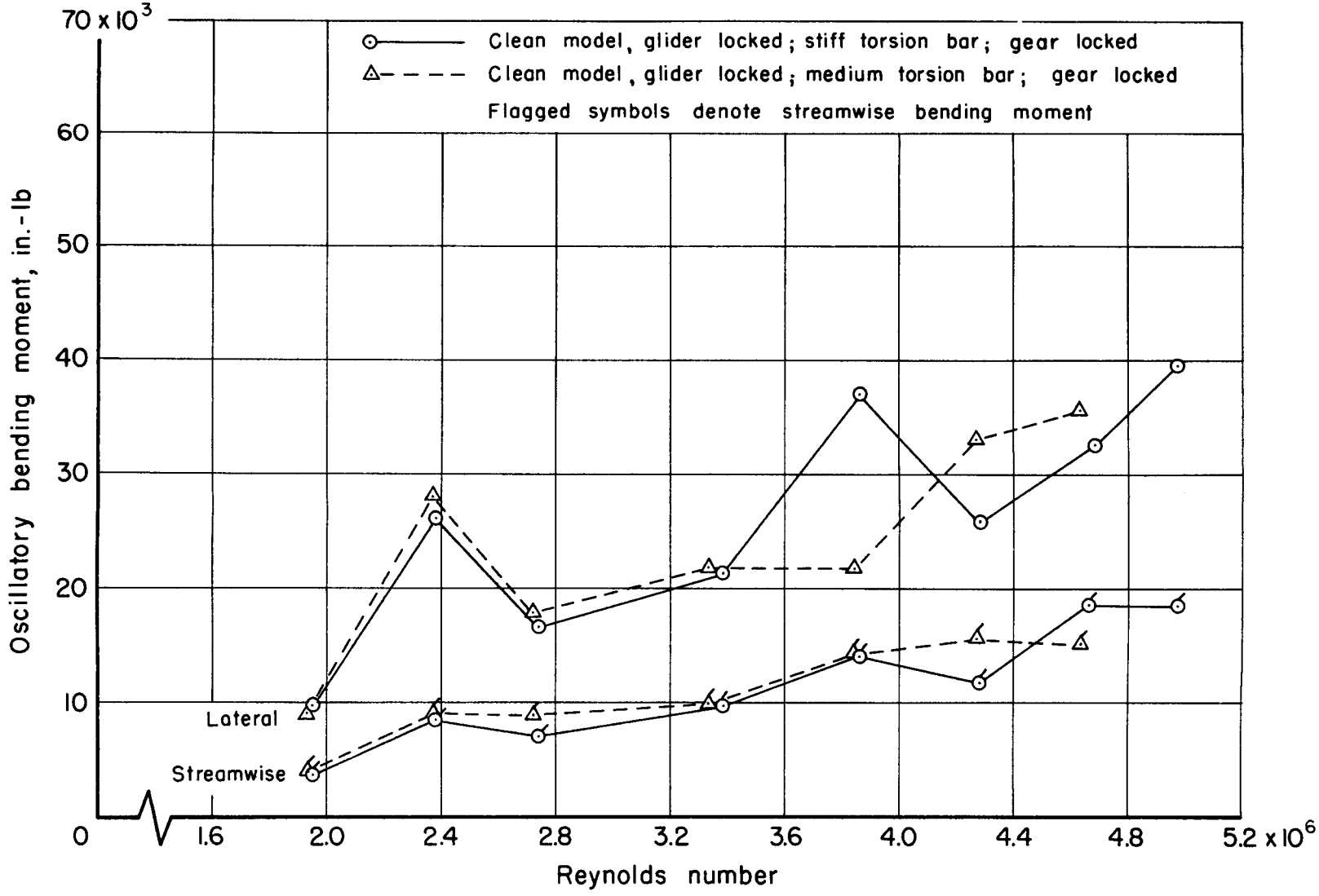

(a) Oscillatory bending moments.

Figure 10.- Glider angle 203°; model clean.

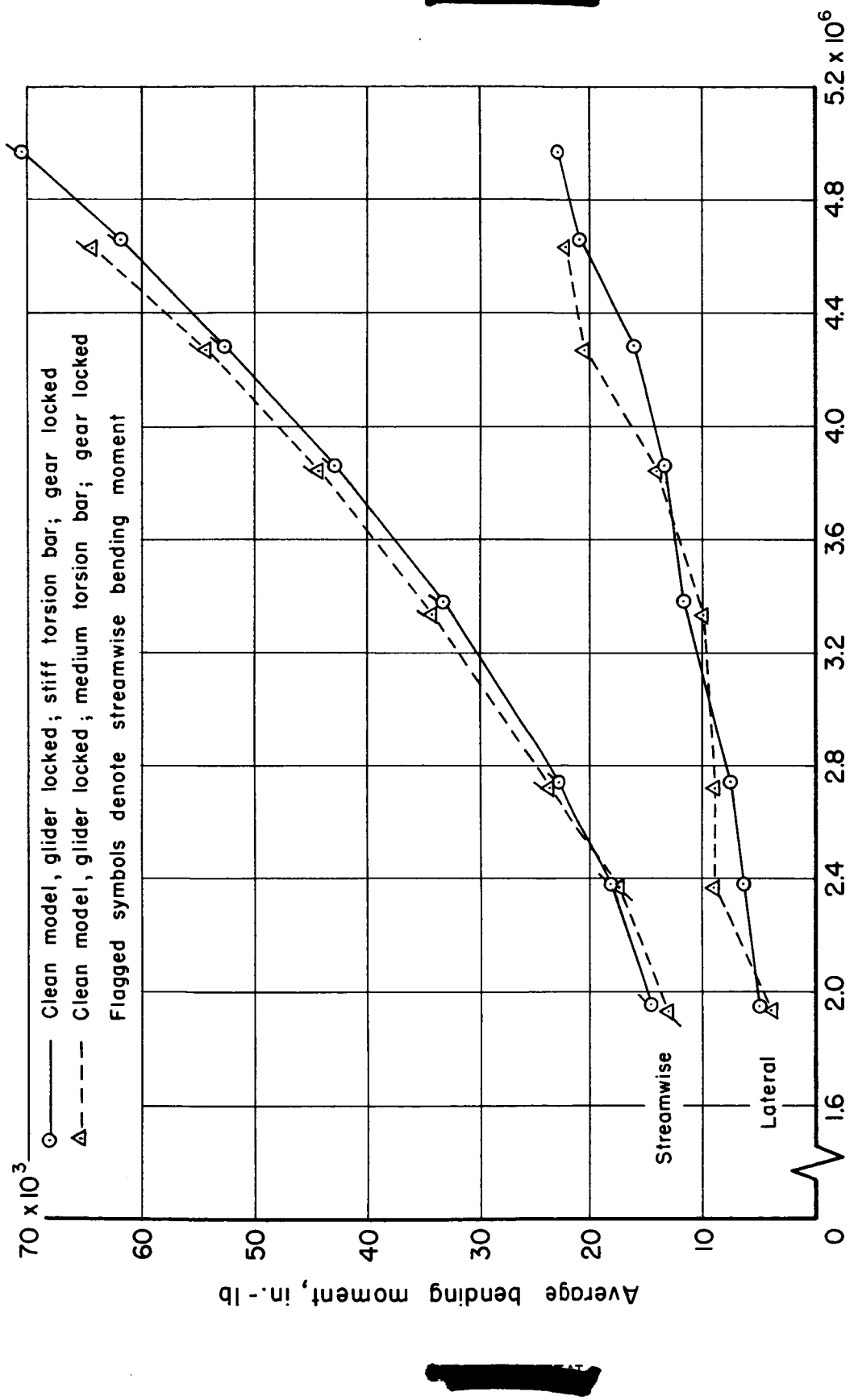

(b) Average bending moments.

Figure 10.- Concluded.

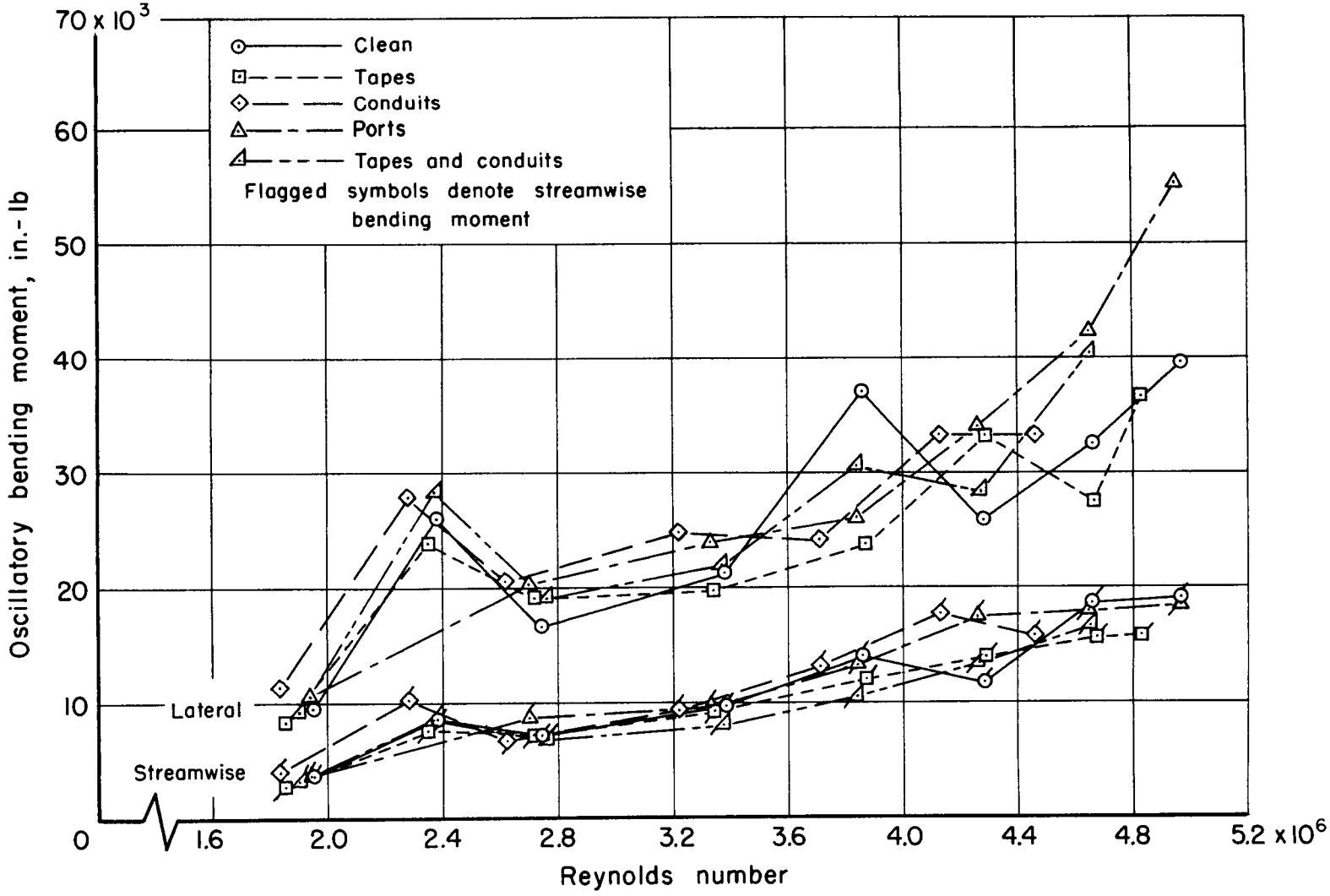

(a) Oscillatory bending moments.

Figure 11.- Effect of surface condition; glider locked at 203°.

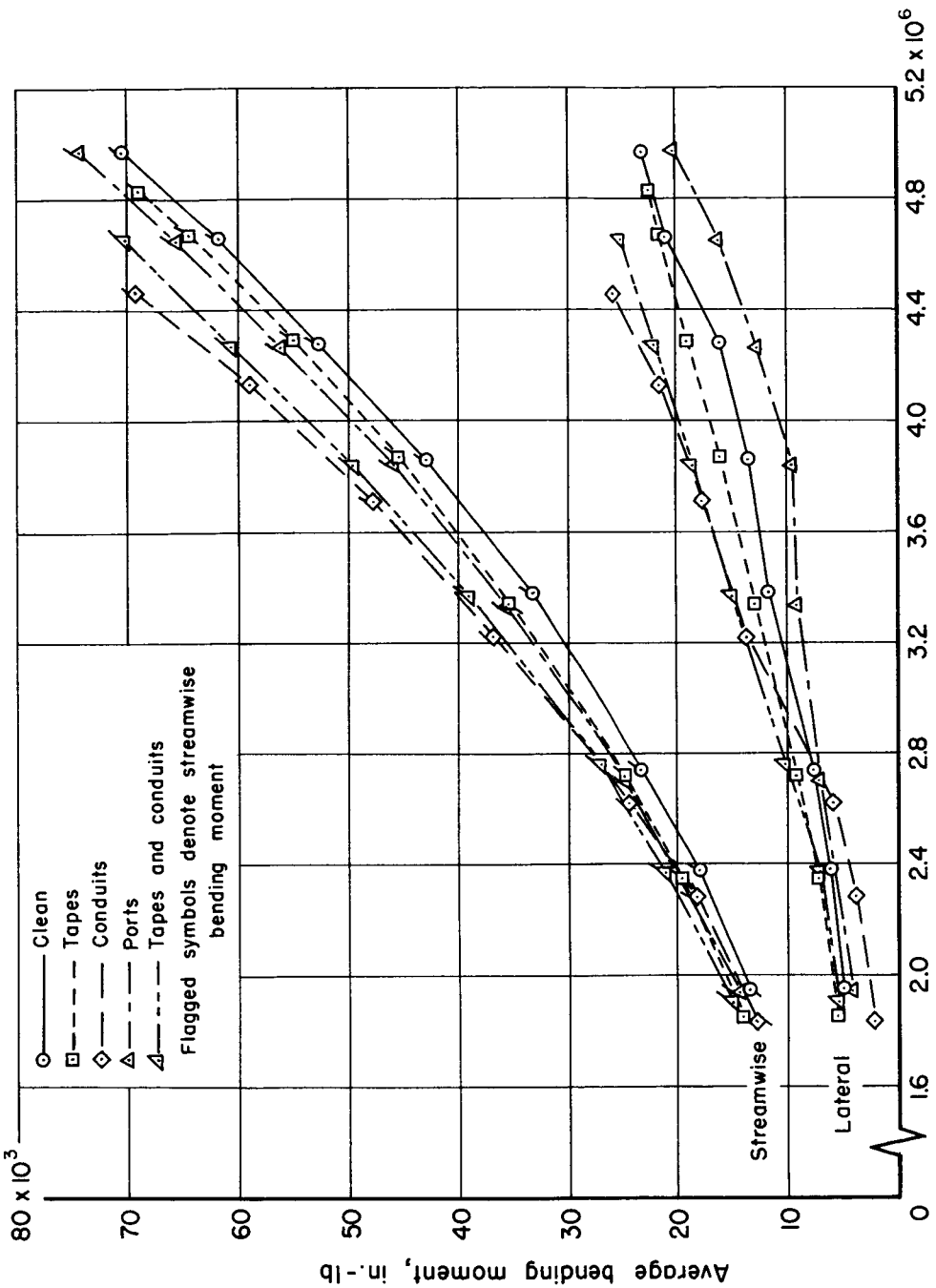

(b) Average bending moments.

Figure 11.- Concluded.

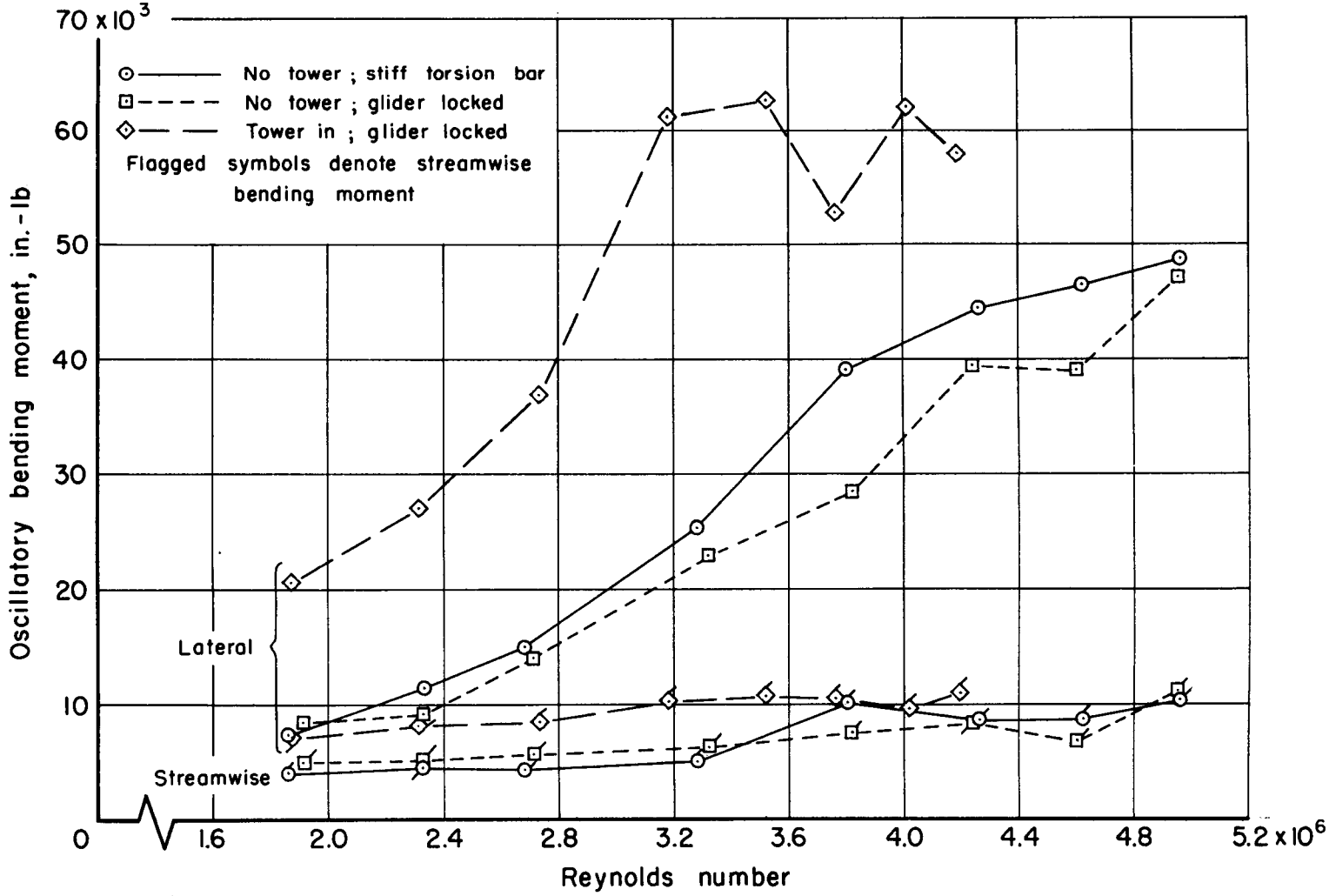

(a) Oscillatory bending moments.

Figure 12.- Effects of glider torsional stiffness and umbilical tower; glider angle 74°, tower angle 29°, model clean.

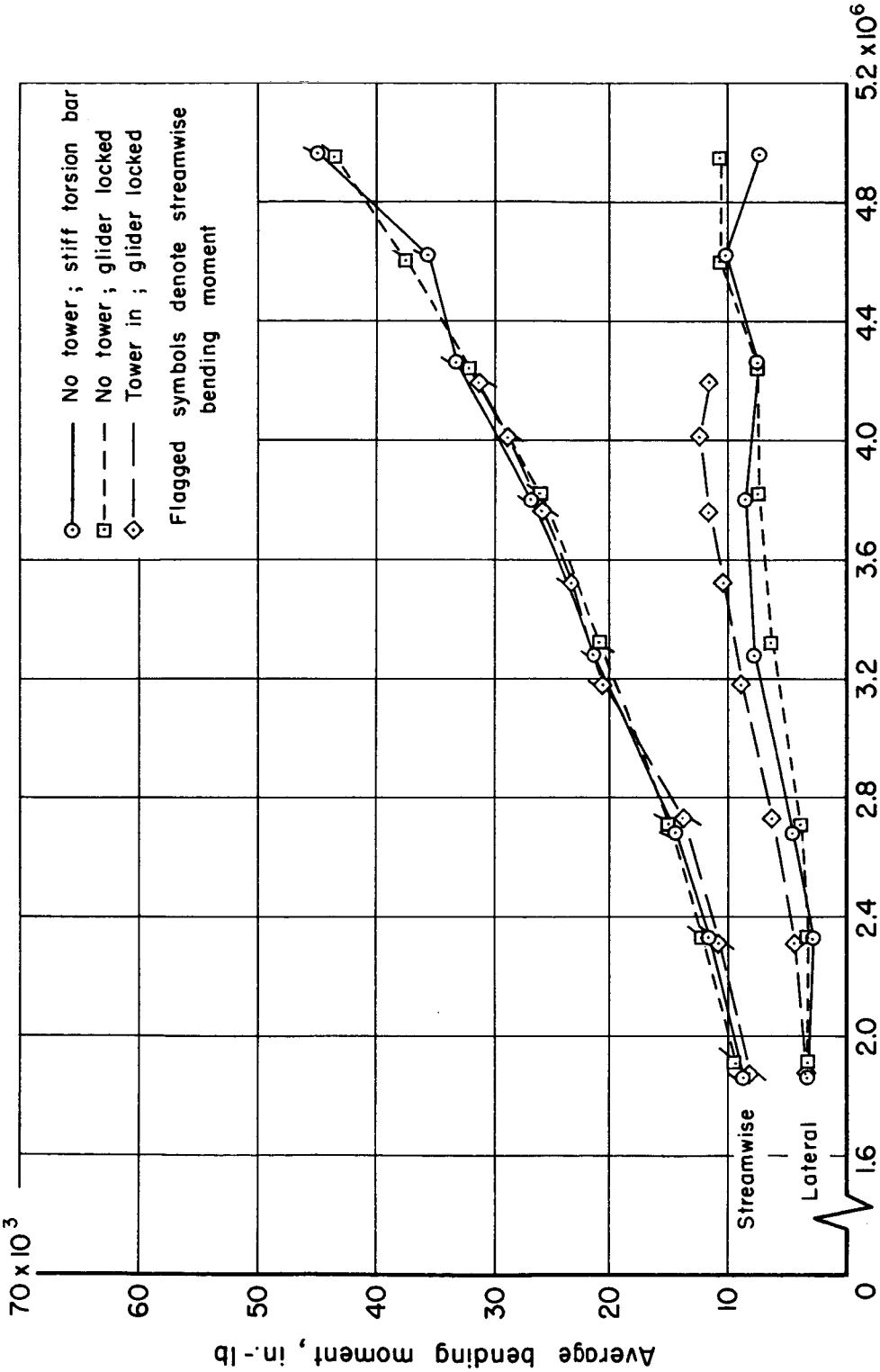

(b) Average bending moments.

Figure 12.- Concluded.

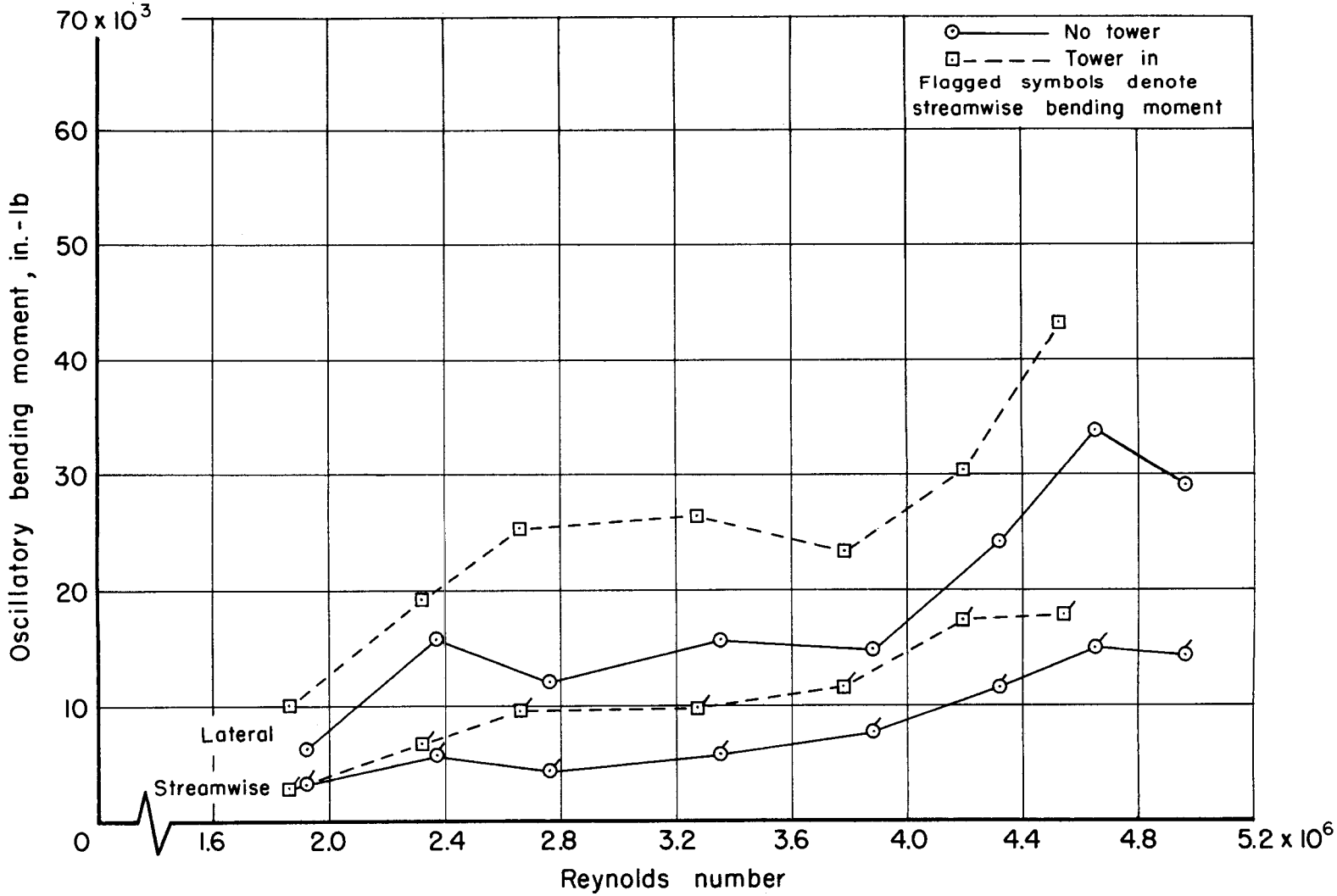

Figure 13.- Effect of umbilical tower; glider angle 203°, tower angle 29°, model clean, gear and glider unlocked.

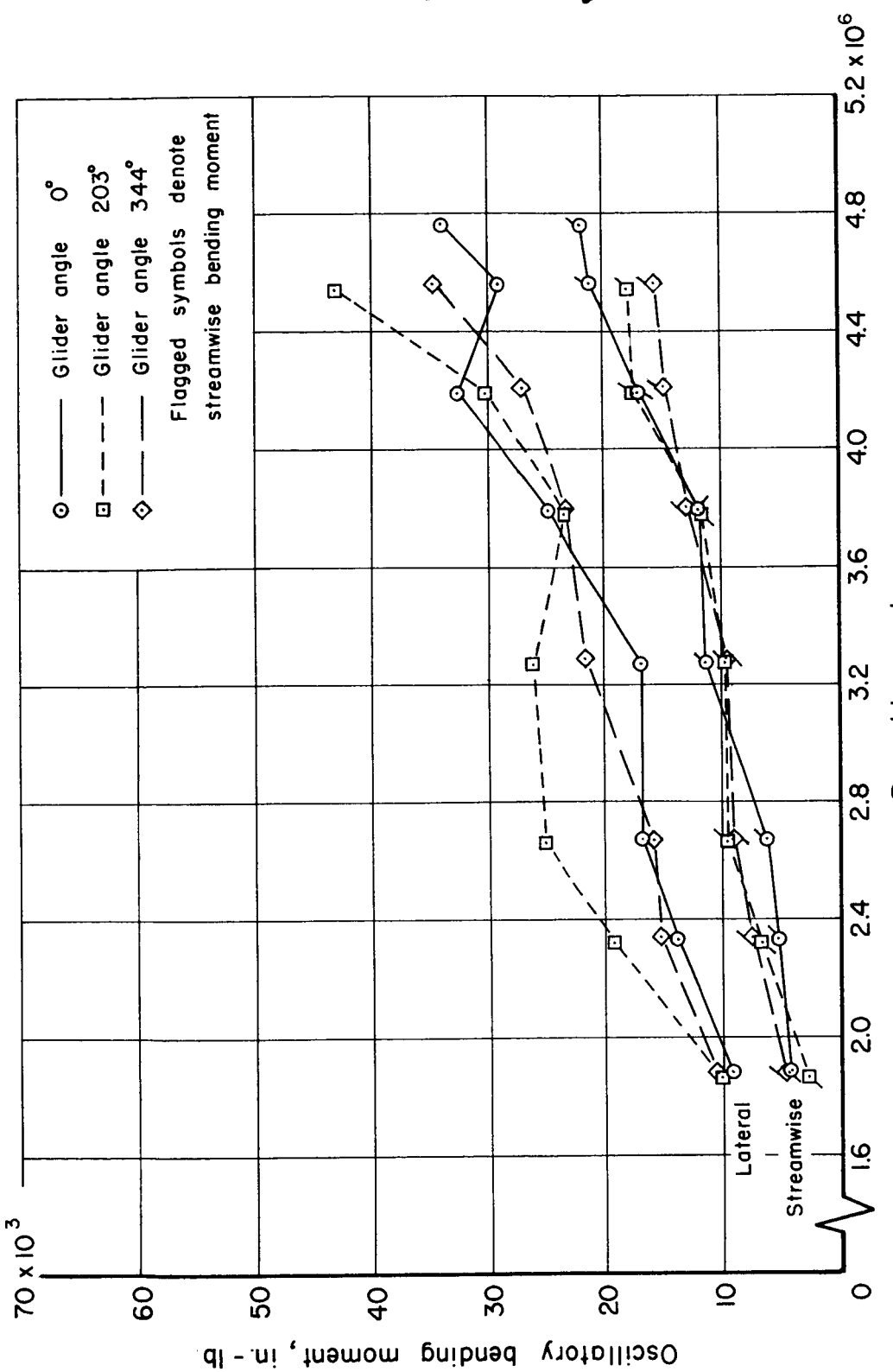

Figure 14.- Effect of glider angle in the presence of the umbilical tower; tower angle 29°, model clean, gear and glider unlocked.

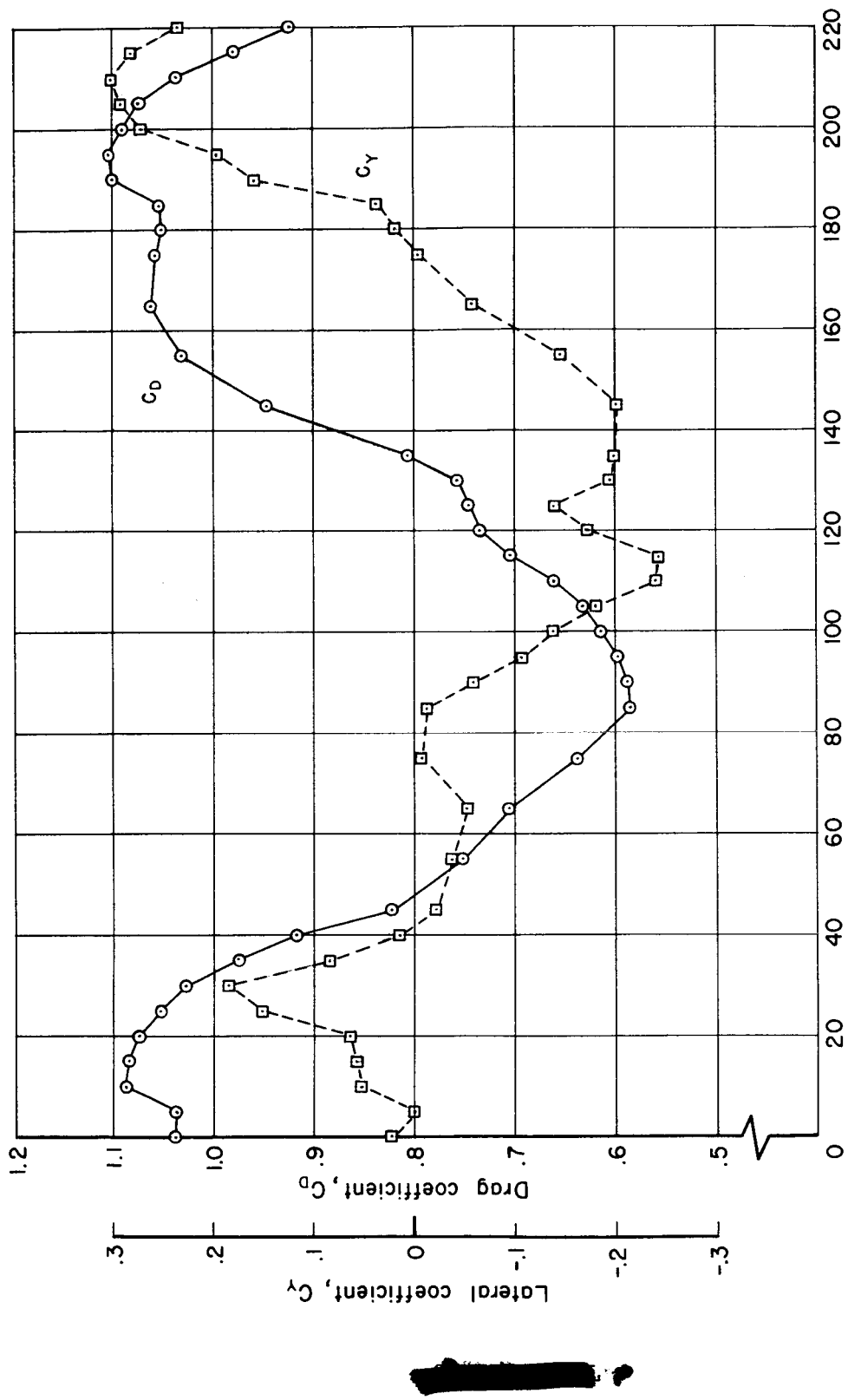

Figure 15.- Static force and moment characteristics of the model with conduits installed and exhaust ports open; Reynolds number 4.5×10^6.

(a) C_D and C_Y

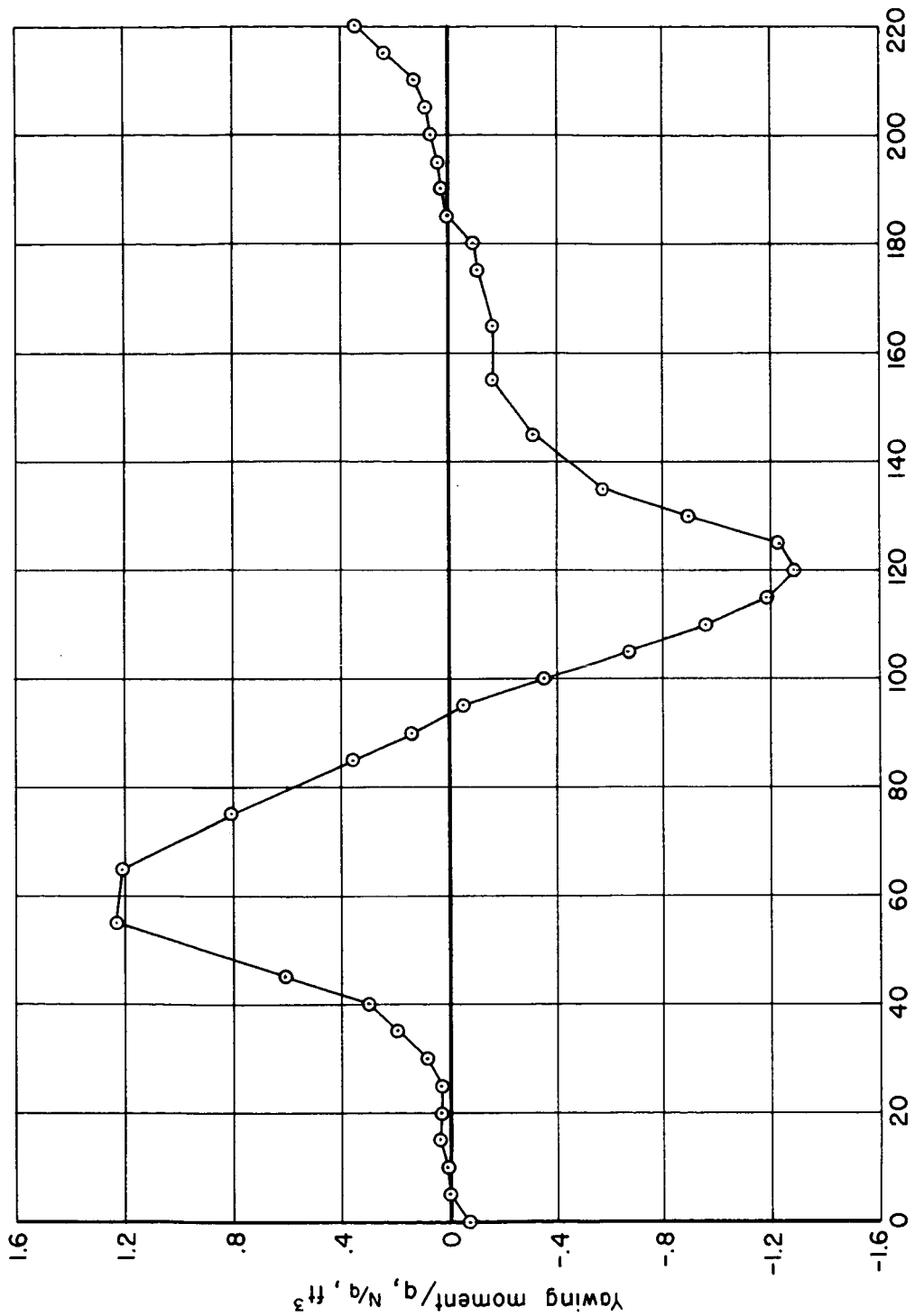

(b) N_q

Figure 15.- Continued.

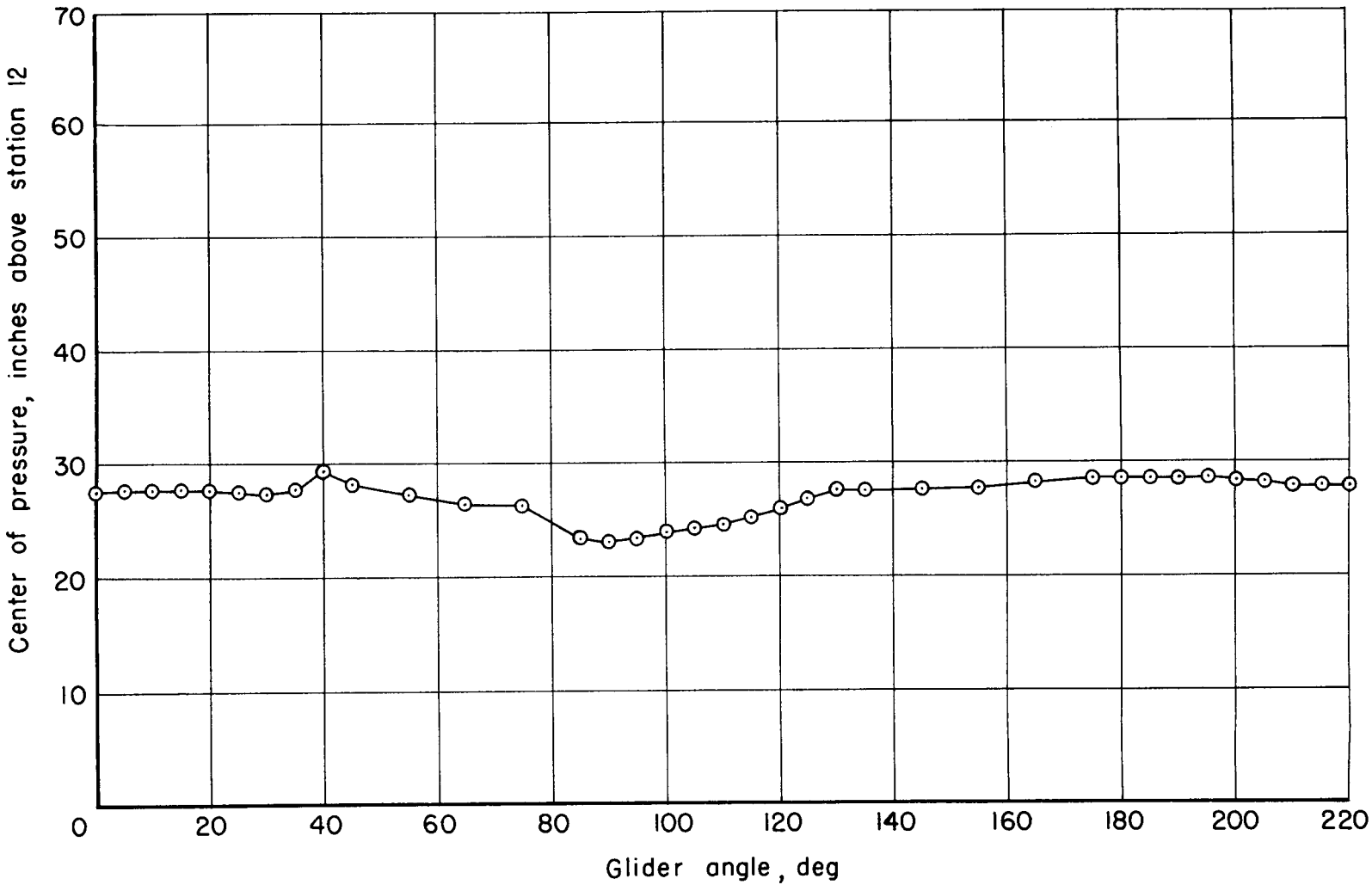

(c) Streamwise center of pressure.

Figure 15.- Continued.

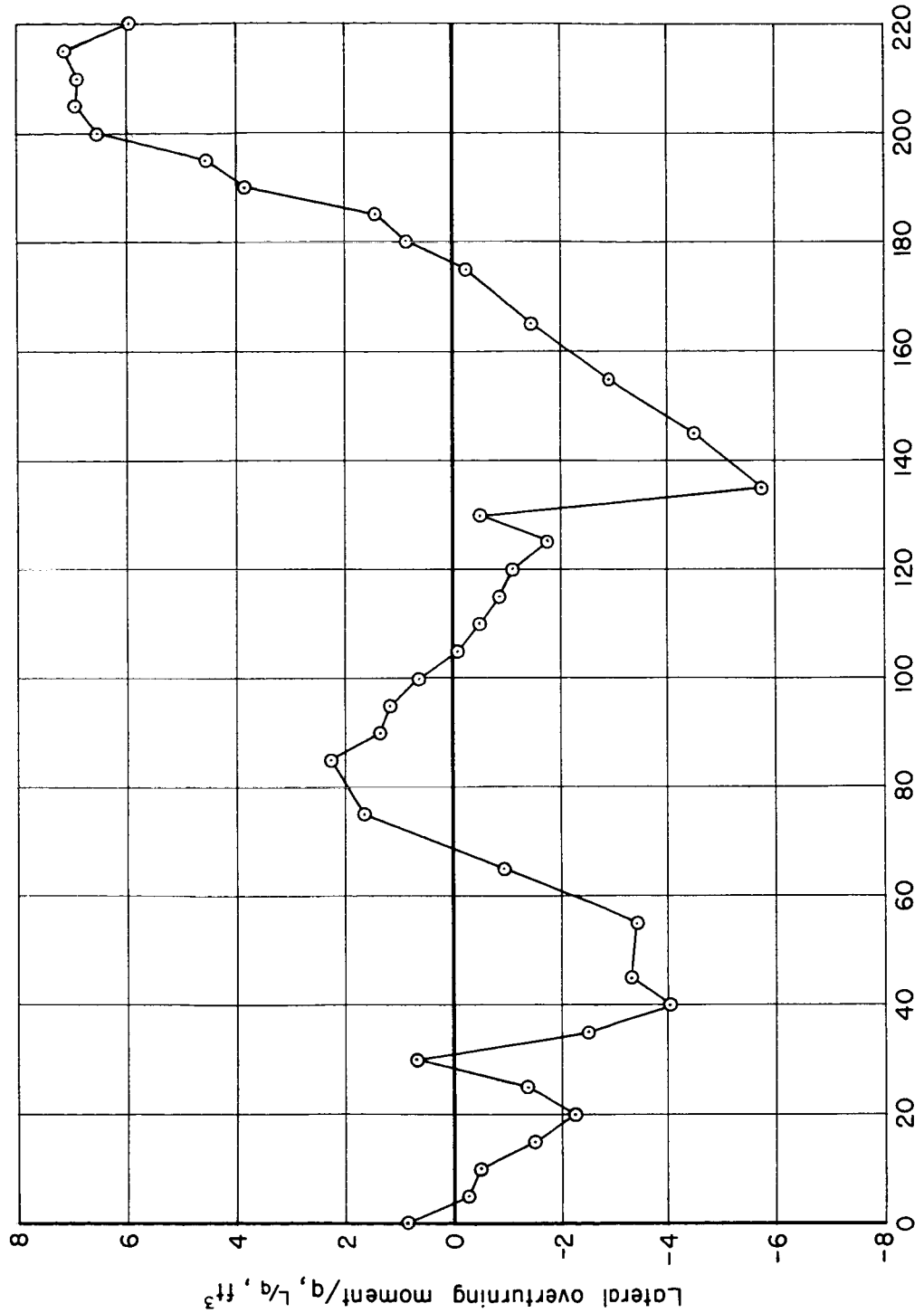

(d) Lateral overturning moment.

Figure 15.- Concluded.

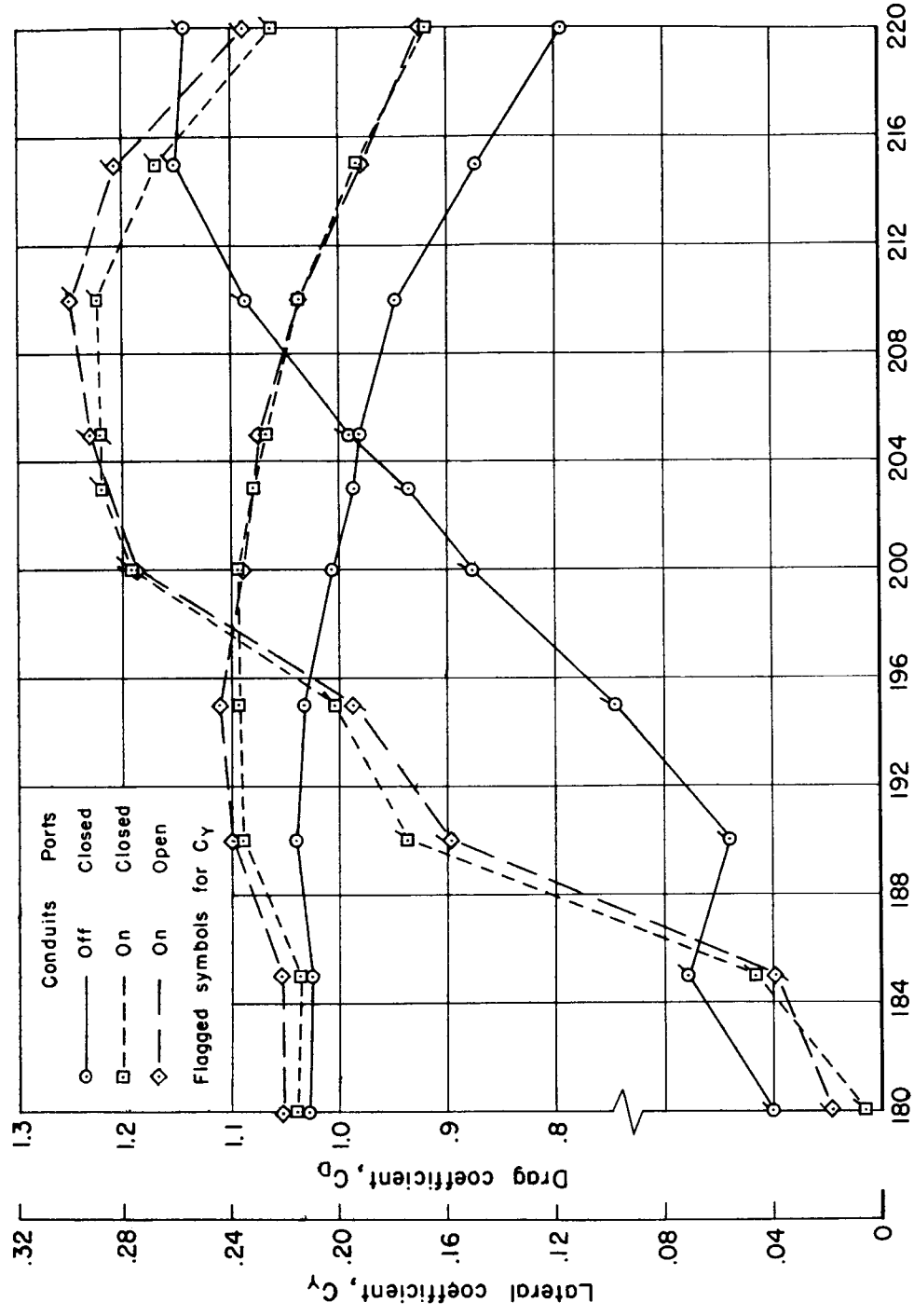

(a) C_D and C_Y

Figure 16.- Effect of conduits and exhaust ports for the angle range 180° to 220°; Reynolds number 4.5×10^6.

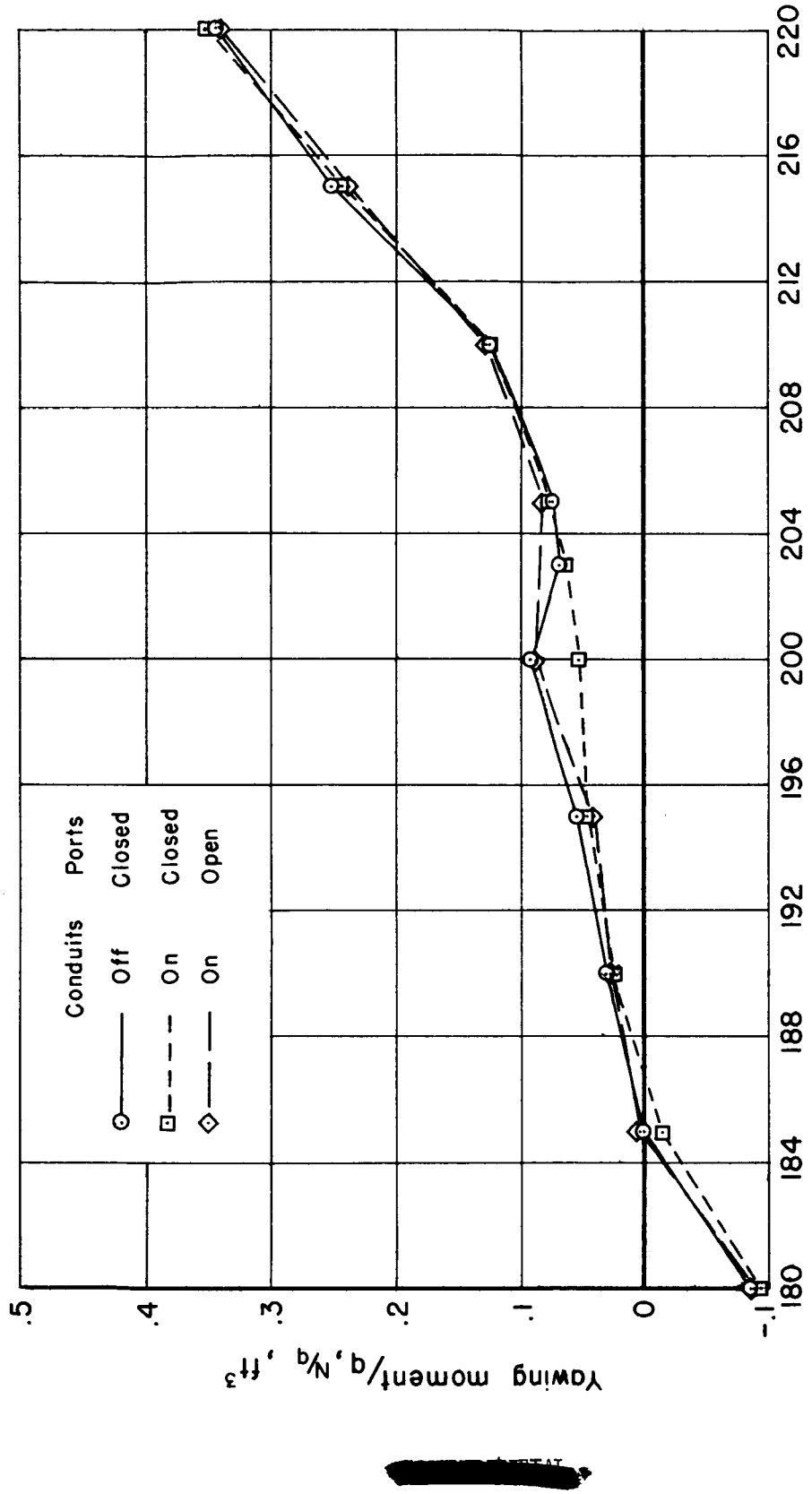

Figure 16.- Continued.

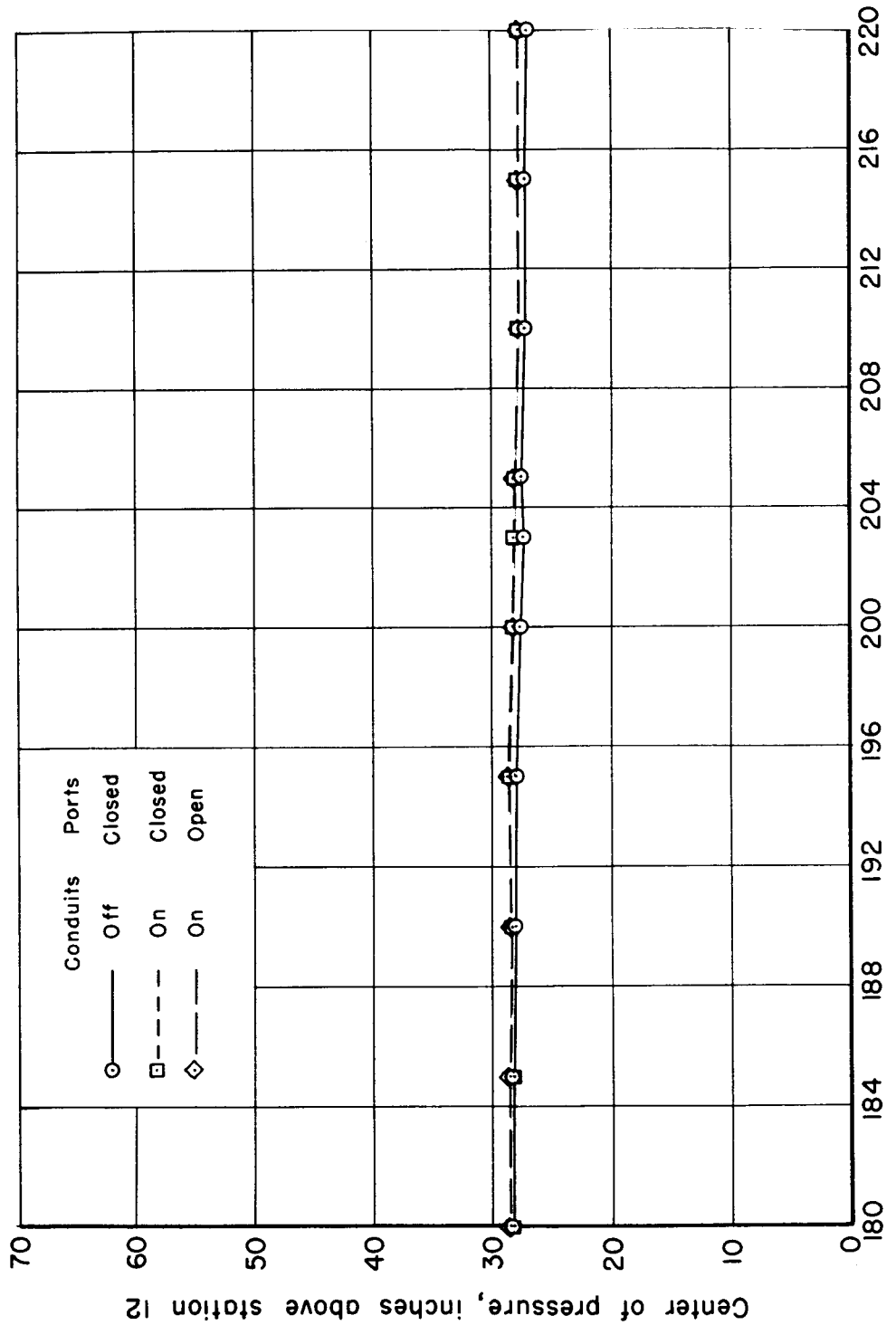

(c) Streamwise center of pressure.

Figure 16.- Continued.

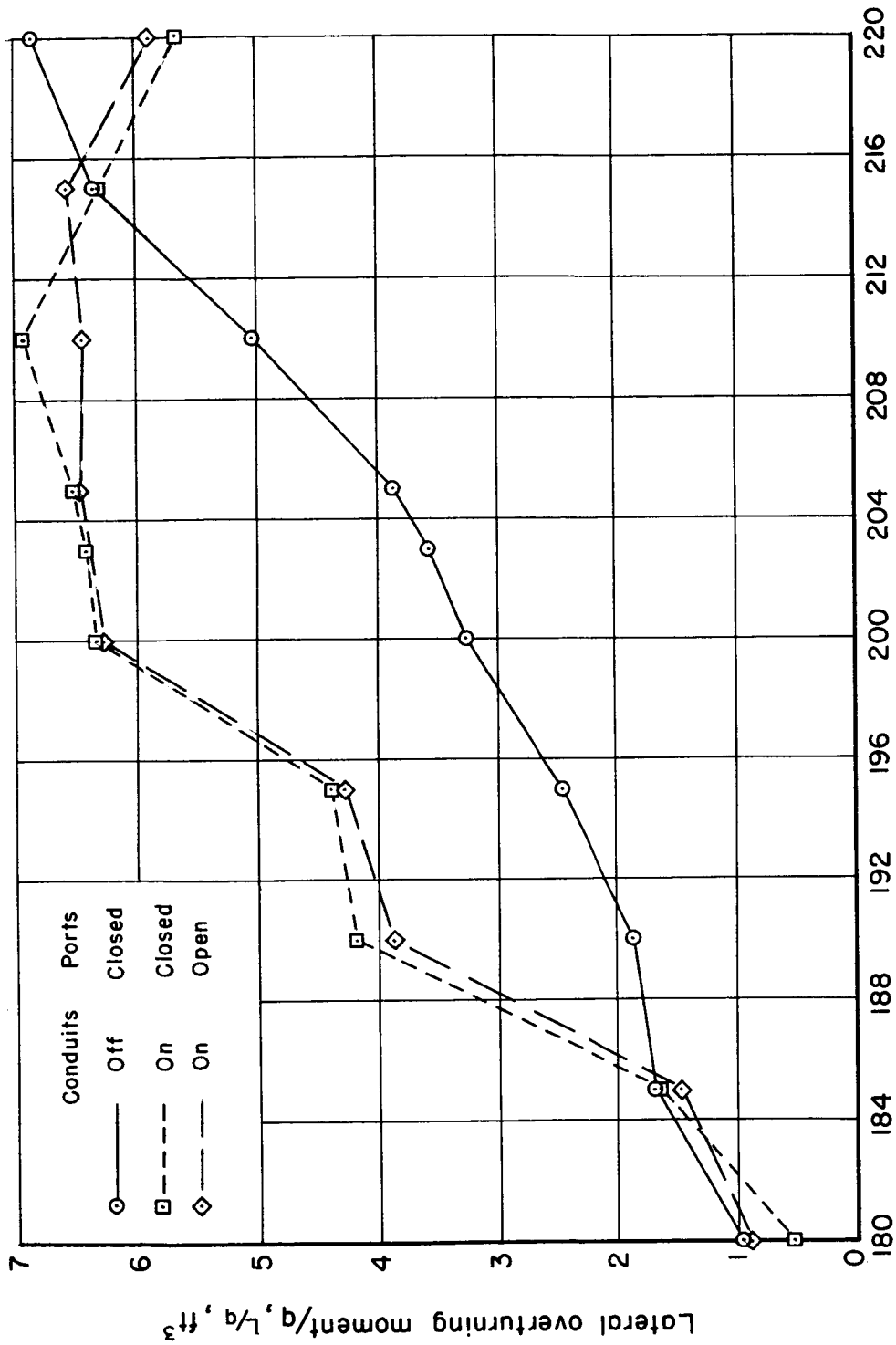

(d) Lateral overturning moment.

Figure 16.- Concluded.

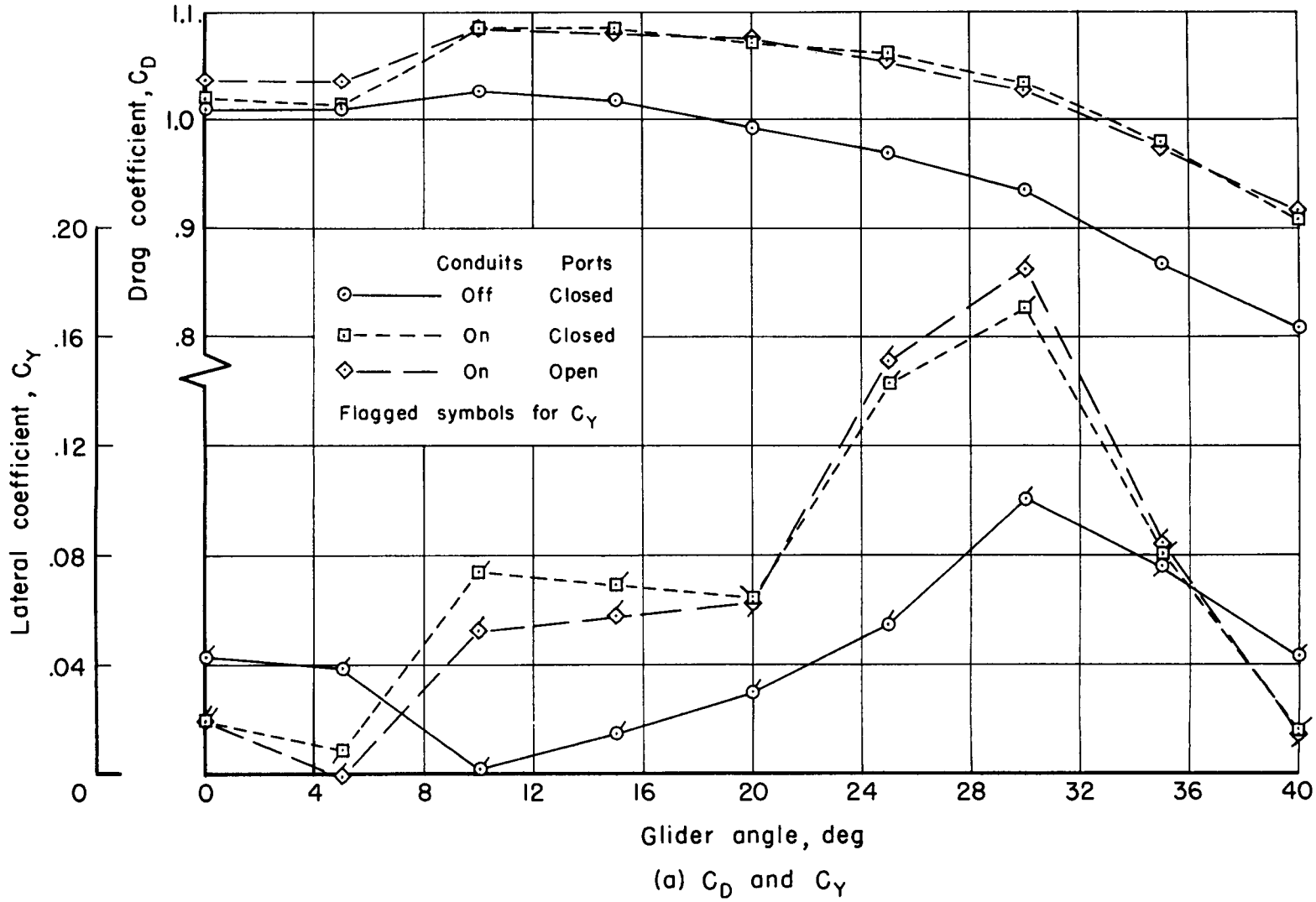

Figure 17.- Effects of conduits and exhaust ports for the angle range 0° to 40°; Reynolds number 4.5×10^6.

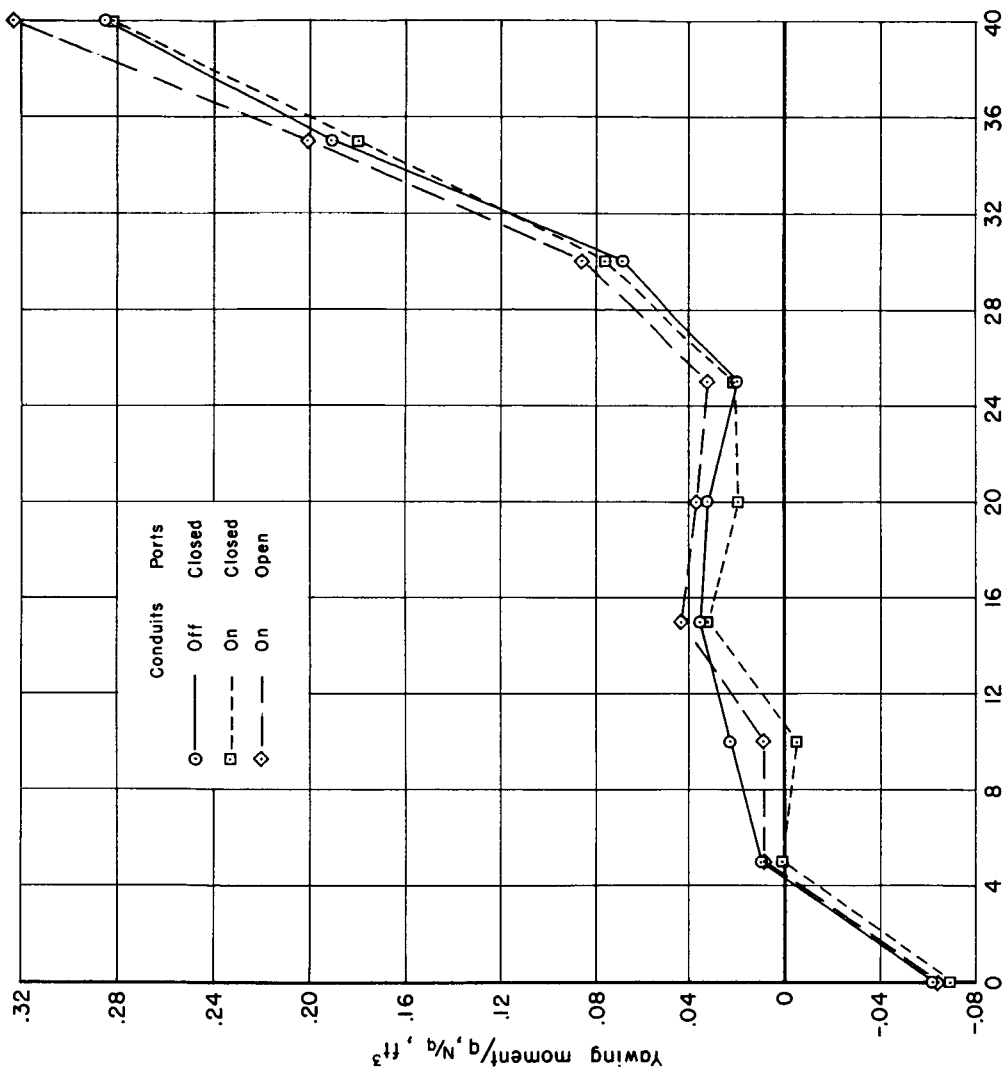

(b) N/q

Figure 17.- Continued.

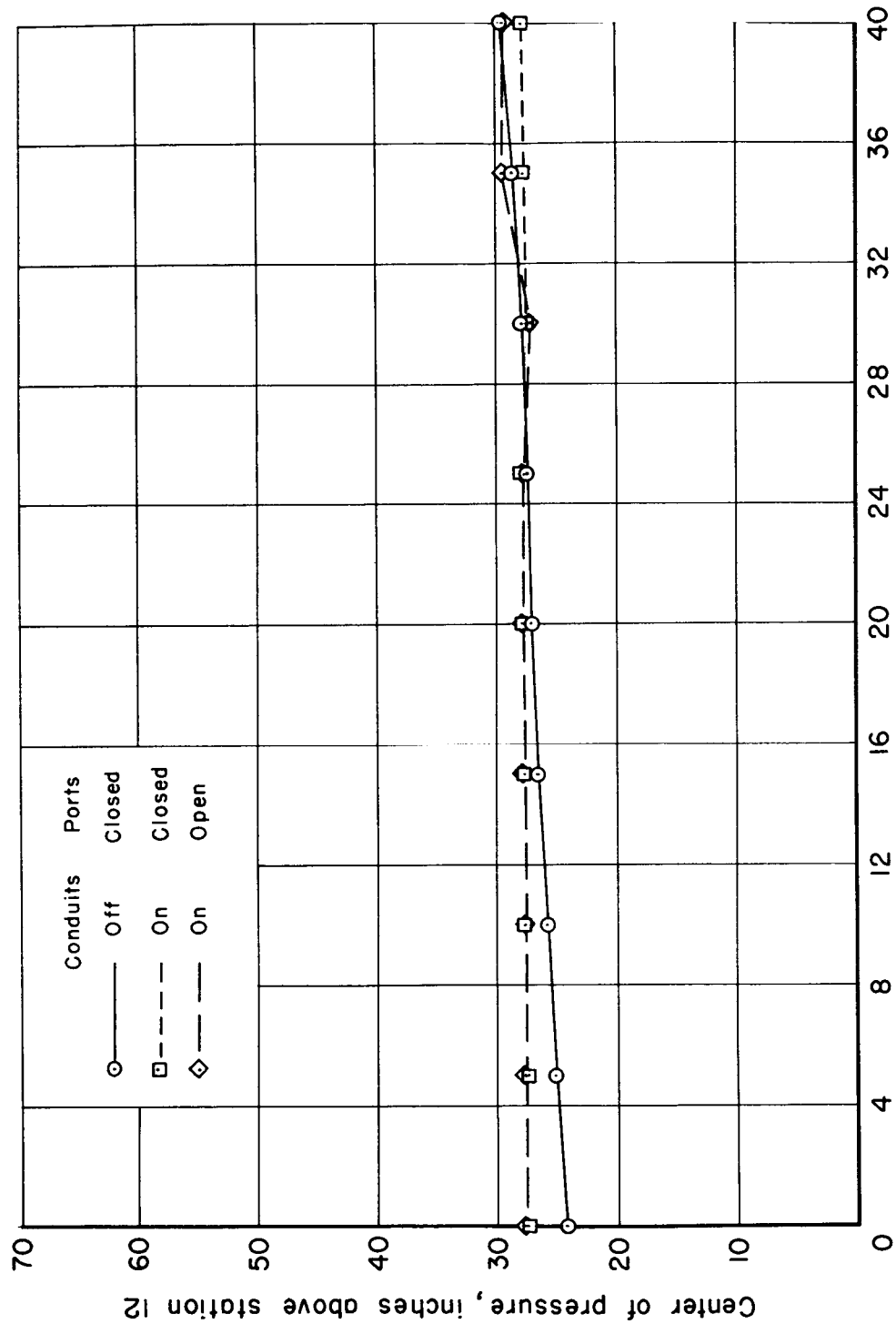

(c) Streamwise center of pressure.

Figure 17.- Continued.

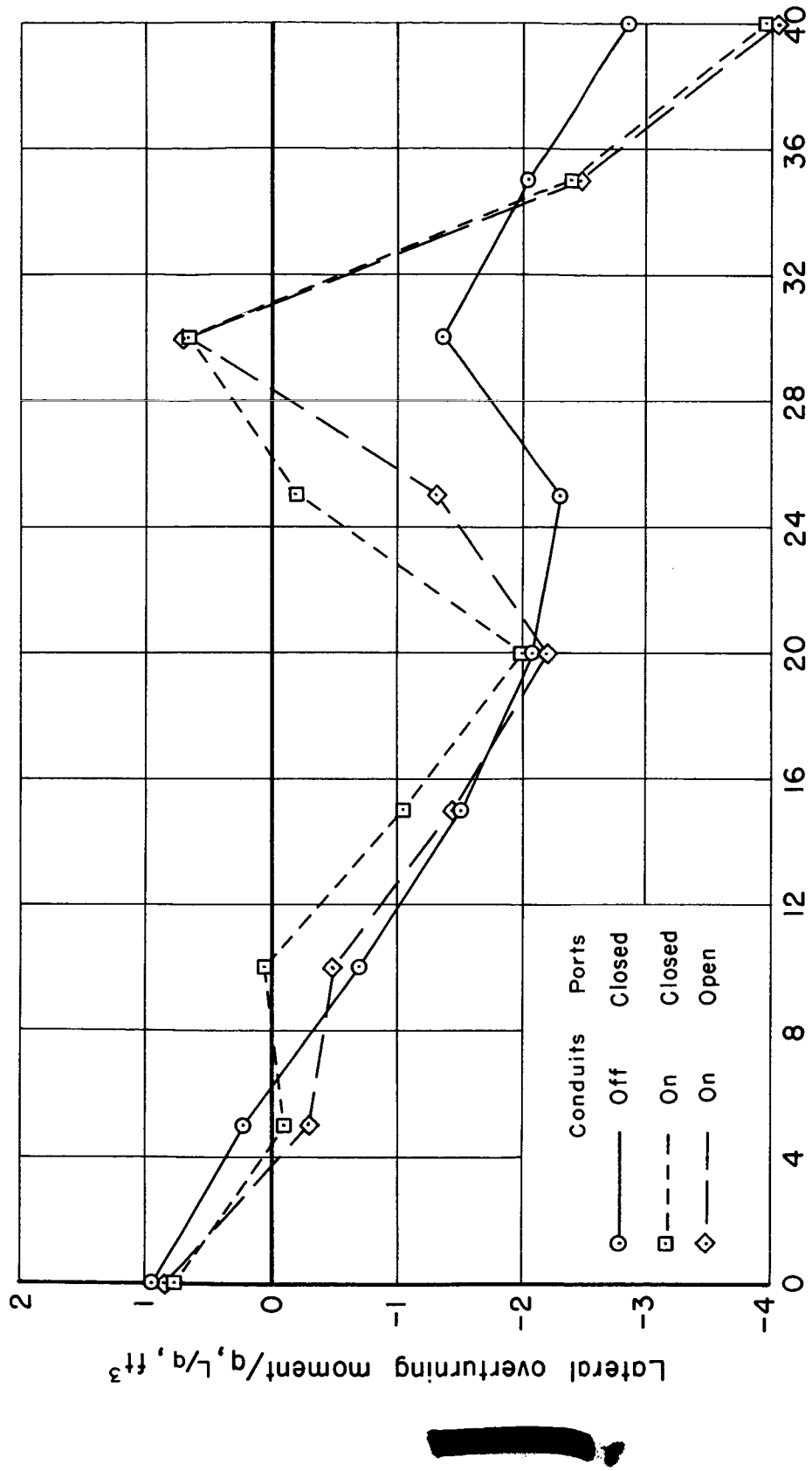

(d) Lateral overturning moment.

Figure 17.- Concluded.

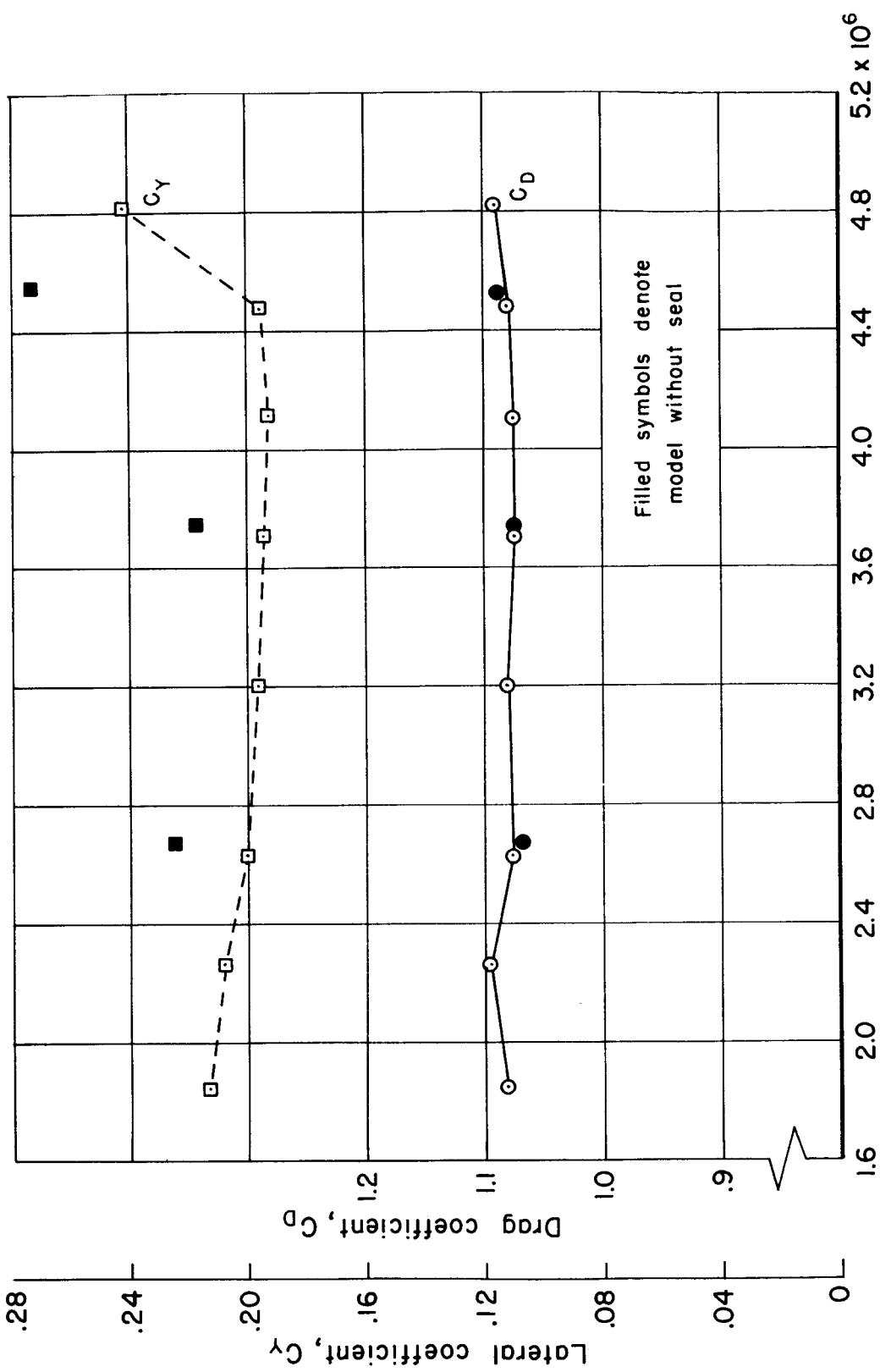

Figure 18.- Effect of Reynolds number for glider and fin angle 200°; model with conduits and exhaust ports open, gap sealed unless otherwise noted.

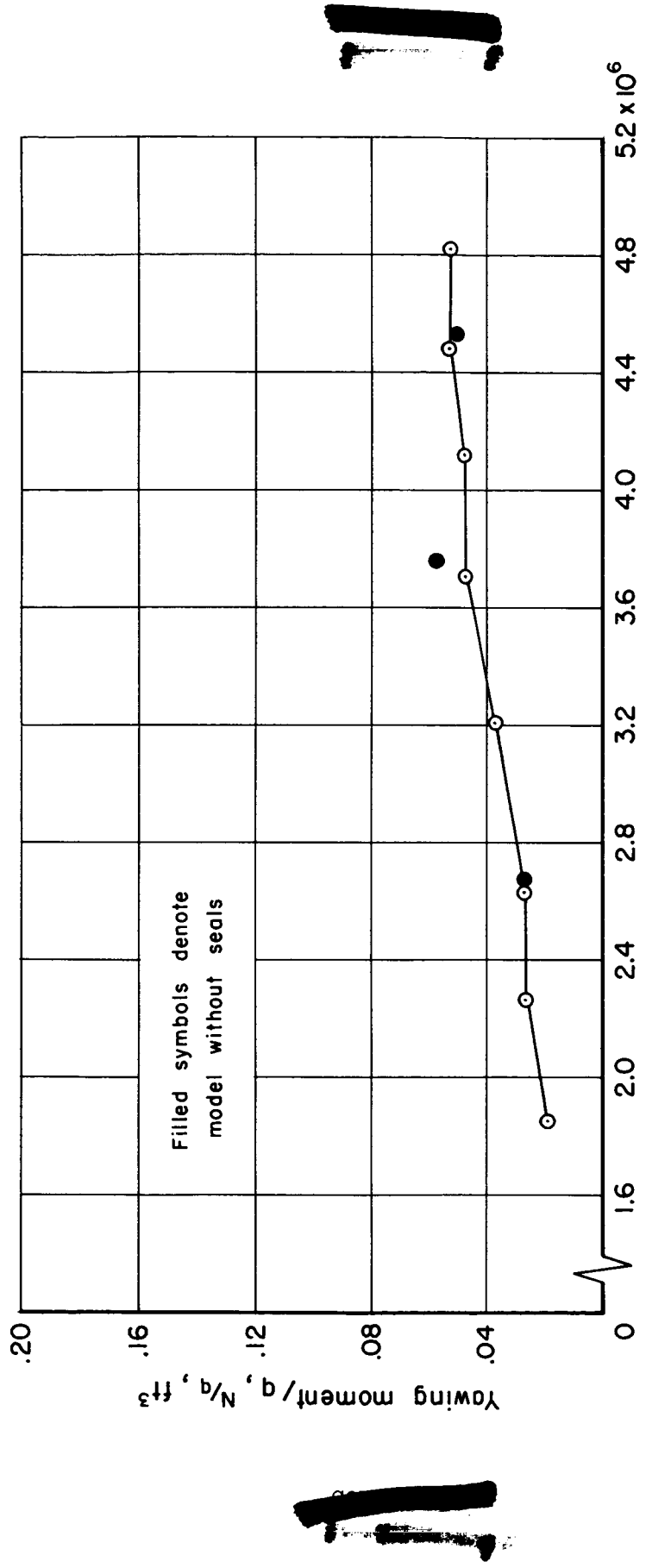

(b) N_q

Figure 18.- Continued.

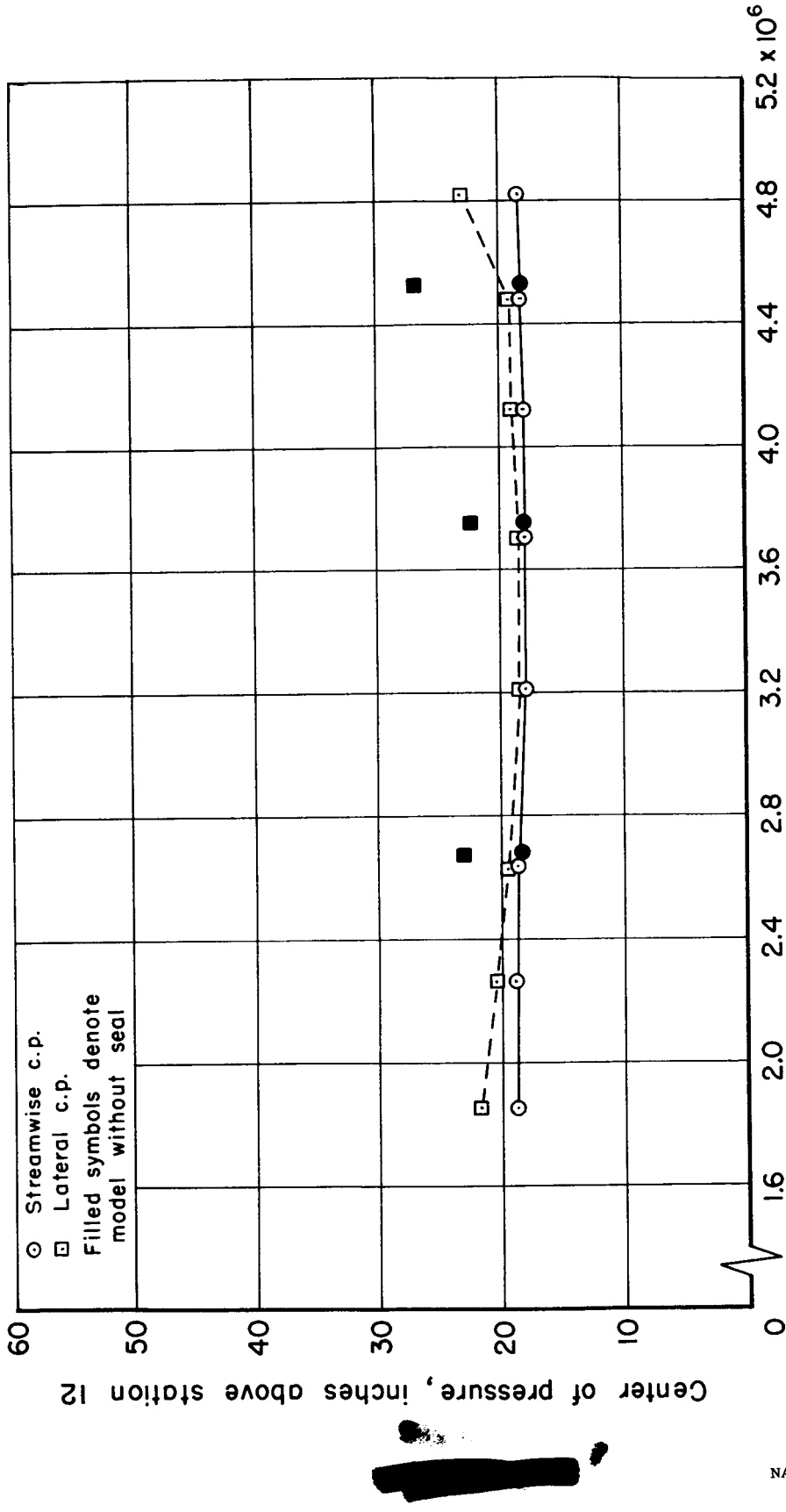

(c) Centers of pressure

Figure 18.- Concluded.

NASA-Langley, 1962 A-606